Clim Dyn
DOI 10.1007/s00382-010-0793-3

Multiproxy summer and winter surface air temperature field reconstructions for southern South America covering the past centuries

R. Neukom · J. Luterbacher · R. Villalba · M. Küttel · D. Frank · P. D. Jones · M. Grosjean · H. Wanner · J.-C. Aravena · D. E. Black · D. A. Christie · R. D'Arrigo · A. Lara · M. Morales · C. Soliz-Gamboa · A. Srur · R. Urrutia · L. von Gunten

Received: 12 November 2009 / Accepted: 8 March 2010

Abstract We statistically reconstruct austral summer (winter) surface air temperature fields back to AD 900 (1706) using 22 (20) annually resolved predictors from natural and human archives from southern South America (SSA). This represents the first regional-scale climate field reconstruction for parts of the Southern Hemisphere at this high temporal resolution. We apply three different reconstruction techniques: multivariate principal component regression, composite plus scaling, and regularized expectation maximization. There is generally good

Electronic supplementary material The online version of this article (doi:10.1007/s00382-010-0793-3) contains supplementary material, which is available to authorized users.

R. Neukom (✉) · M. Küttel · M. Grosjean · H. Wanner · L. von Gunten
Oeschger Centre for Climate Change Research (OCCR), University of Bern, Bern, Switzerland
e-mail: neukom@giub.unibe.ch

R. Neukom · M. Küttel · M. Grosjean · H. Wanner · L. von Gunten
Institute of Geography, Climatology and Meteorology, University of Bern, Bern, Switzerland

J. Luterbacher
Department of Geography; Climatology, Climate Dynamics and Climate Change, Justus Liebig University of Giessen, Giessen, Germany

R. Villalba · M. Morales · A. Srur
Instituto Argentino de Nivología, Glaciología y Ciencias Ambientales (IANIGLA), CONICET, Mendoza, Argentina

M. Küttel
Department of Earth and Space Sciences, University of Washington, Seattle, USA

D. Frank
Swiss Federal Research Institute WSL, 8903 Birmensdorf, Switzerland

P. D. Jones
Climatic Research Unit, School of Environmental Sciences, University of East Anglia, Norwich, UK

J.-C. Aravena
Centro de Estudios Cuaternarios de Fuego Patagonia y Antártica (CEQUA), Avenida Bulnes 01890, Punta Arenas, Chile

D. E. Black
School of Marine and Atmospheric Sciences, Stony Brook University, Stony Brook, USA

D. A. Christie · A. Lara · R. Urrutia
Laboratorio de Dendrocronología, Facultad de Ciencias Forestales y Recursos Naturales, Universidad Austral de Chile Valdivia, Casilla 567, Valdivia, Chile

R. D'Arrigo
Tree-Ring Laboratory, Lamont-Doherty Earth Observatory, Earth Institute at Columbia University, Palisades, NY, USA

A. Lara
Núcleo Científico Milenio FORECOS, Fundación FORECOS, Valdivia, Chile

C. Soliz-Gamboa
Section of Ecology and Biodiversity, Faculty of Science, Institute of Environmental Biology, Utrecht University, P.O. Box 80084, 3508 TB Utrecht, The Netherlands

L. von Gunten
Department of Geosciences, Climate System Research Center, University of Massachusetts, Amherst, USA

Published online: 28 March 2010

agreement between the results of the three methods on interannual and decadal timescales. The field reconstructions allow us to describe differences and similarities in the temperature evolution of different sub-regions of SSA. The reconstructed SSA mean summer temperatures between 900 and 1350 are mostly above the 1901–1995 climatology. After 1350, we reconstruct a sharp transition to colder conditions, which last until approximately 1700. The summers in the eighteenth century are relatively warm with a subsequent cold relapse peaking around 1850. In the twentieth century, summer temperatures reach conditions similar to earlier warm periods. The winter temperatures in the eighteenth and nineteenth centuries were mostly below the twentieth century average. The uncertainties of our reconstructions are generally largest in the eastern lowlands of SSA, where the coverage with proxy data is poorest. Verifications with independent summer temperature proxies and instrumental measurements suggest that the interannual and multi-decadal variations of SSA temperatures are well captured by our reconstructions. This new dataset can be used for data/model comparison and data assimilation as well as for detection and attribution studies at sub-continental scales.

Keywords Climate change · Climate field reconstructions · Temperature · South America

1 Introduction

Understanding the current and future processes and dynamics of the climate system requires knowledge of the spatial patterns, trends, amplitudes and frequencies of climatic variations including information from the past (Jansen et al. 2007; Jones et al. 2009; Mann et al. 2008). While instrumental records (e.g. Brohan et al. 2006) provide insights into climate variability of the recent anthropogenically forced climate system, they are often too short to allow assessment of the natural modes of climatic variations. In this regard, proxy data—records which serve as a surrogate for instrumental measurements—have allowed climate variations to be evaluated over the past centuries to millennia (see e.g., Jones et al. 2009 for a review). Climate reconstructions provide insight into the mechanisms or forcings underlying observed climate variability and are of importance for data/climate model comparisons.

Until recently, the rather low number and uneven spatial distribution of temporally-highly-resolved proxies from the Southern Hemisphere (SH) did not allow reliable continental scale reconstructions to be developed at interannual to interdecadal time scales (Jansen et al. 2007; Mann and Jones 2003). Consequently, the few existing multi-proxy temperature reconstructions from the SH focus on the hemispheric mean (Jones et al. 1998; Mann and Jones 2003; Mann et al. 2008) and depend upon on a small number of SH proxies (see e.g., Ljungqvist 2009 and references therein). Accordingly, these reconstructions do not provide reliable representations of the spatial patterns, trends and amplitudes of regional to continental scale SH climate. However, reconstructions of high spatial and temporal resolution are important, because they illuminate key climatic features, such as regionally very hot/cool seasonal conditions that may be masked in a hemispheric reconstruction. The limited understanding of SH climate is particularly striking given the importance of understanding the potential see-saw mechanisms between the climatic state of the Northern Hemisphere (NH) versus SH continents on interannual to millennial time scales as well as the crucial role of the SH oceans in regulating global climate variability (e.g., Busalacchi 2004).

South America is a key region for the understanding of Southern Hemisphere climate dynamics, as it is the only landmass that extends from the tropics to latitudes poleward of 50°S. It is influenced by a variety of atmospheric and oceanic patterns, including globally relevant large-scale modes such as the El Niño Southern Oscillation (ENSO), the Southern Annular Mode (SAM) and the Pacific Decadal Oscillation (PDO; Garreaud et al. 2009). Furthermore, South America's climate is strongly affected and modulated by the continuous Cordillera of the Andes in the west and the large Amazon basin in the northeast.

Due to the still very limited number of highly resolved paleoclimatic records from the tropical part of South America (Villalba et al. 2009), this study focuses on southern South America (SSA, south of 20°S).

The largest fraction of the published paleoclimatic information from SSA is represented by Andean tree rings (see Boninsegna et al. 2009 for a review). Annually resolved temperature reconstructions on local to regional scale have been developed using tree rings from southern Patagonia and Tierra del Fuego back to 1650 (Aravena et al. 2002; Boninsegna et al. 1989; Villalba et al. 2003) as well as from northern Patagonia, where the longest tree ring records extend back more than 3,500 years (Lara and Villalba 1993; Villalba 1990; Villalba et al. 1997a, 2003). New records from ice cores (Vimeux et al. 2009 and references therein) and lake sediments (e.g. von Gunten et al. 2009) complement the network of temporally highly resolved natural proxies from SSA. The regional temperature history of the subtropical Andes has been investigated based on the lake sediment record from Laguna Aculeo (von Gunten et al. 2009), covering the period 857–2003. In addition to the natural proxies, several documentary records are available, most of them originating from subtropical SSA (e.g. Neukom et al. 2009; Prieto and García

Herrera 2009). Along with proxies from outside SSA, that are connected to the South American climate via teleconnections, the data now allow us to establish an extensive set of climate predictors for past SSA climate. On centennial timescales, glacier length records from the Andes also provide insight into the climate history of SSA (Koch and Kilian 2005; Luckman and Villalba 2001; Masiokas et al. 2009; Villalba 1994).

In this work, we present the first SSA austral summer (DJF) and winter (JJA) temperature field reconstructions. Out of an extended set of 144 annually resolved SSA climate proxies we select 22 (20) predictors for the summer (winter) reconstructions. Three different techniques were applied to statistically reconstruct the SSA mean as well as spatial temperature fields. Proxy data were sufficient to reconstruct winter temperatures back to 1706 and summer temperatures back to 900.

2 Data and methods

2.1 Instrumental calibration data

We used the new monthly and 0.5° × 0.5° resolved CRU TS 3 temperature grid covering 1901–2006 (updated from Mitchell and Jones 2005) as a predictand for the reconstructions (see Sect. 2.3 for methodological details). Seasonal values were calculated by averaging the austral summer (December to February, DJF) and winter (June to August, JJA) months, respectively. We selected this traditional definition of the seasons, because the combination of these months represents a compromise with respect to the varying temperature sensitivities of the different proxy records. We defined the reconstruction area (SSA) as the terrestrial area between 20°S and 55°S and between 30°W and 80°W, covered by a total of 2,358 (land-) grid boxes.

2.2 Predictor data

As a basis for the proxy evaluation and temperature reconstruction, we compiled 144 proxies, which are sensitive to SSA climate (Tables S1–S3 in the supplementary material). The dataset includes records from natural archives (tree rings, lake and marine sediments, ice cores and corals), documentary evidence and a set of homogenized instrumental temperature measurements. Some of the records were additionally processed as described in the supplementary material. Due to the limited number of long proxies from SSA, we also included records from distant areas into our predictor sets. Earlier studies based on instrumental measurements (e. g. Dettinger et al. 2001; Garreaud and Battisti 1999; Garreaud et al. 2009; Villalba et al. 1997b) revealed that these regions are related to SSA climate via teleconnections, mainly SAM and ENSO, and can explain significant fractions of SSA summer and winter temperature variability. Together, ENSO and SAM explain 38% of annual SSA mean temperature variability 1950–2006. The spatial correlations of SSA summer and winter temperatures with ENSO and SAM are shown in Fig. S1 in the supplementary material. However, we are aware that the inclusion of the proxies from distant areas may bias the reconstruction results, because the teleconnections patterns relating them to SSA climate may not be stable through time. Recent studies from Europe showed that the quality and location of predictors is probably more important for reliable reconstructions than the total number of predictors (Küttel et al. 2007; von Storch et al. 2009). Working in this direction, we assessed the quality and value of each proxy individually, finally reducing our predictor set to 22 (20) summer (winter) temperature proxies. As selection criteria we used the change in predictive skill of the predictor set within the verification period, when a candidate series is added to/removed from a previous set (detailed description of the procedure see supplementary material). An overview of the finally selected records and their temporal span is provided in Tables 1 and 2 and Fig. 1. The optimized set for summer consists of 16 records from within SSA (data sources see Table 1): 11 tree ring chronologies, mainly from the Patagonian Andes, a lake sediment record from central Chile, and 4 long instrumental temperature time series. The set is completed by six proxies from outside SSA: a marine sediment record from the Cariaco Basin off Venezuela, δ^{18}O and accumulation series from the Quelccaya ice core, a tree ring based temperature reconstruction from New Zealand, and two coral records from Australian coastal waters. For the winter temperature reconstructions, the optimized proxy set (data sources see Table 2) contains four tree ring, two documentary, and three instrumental records from within SSA. Proxy data from outside SSA include: a tree ring record from the Bolivian Altiplano, a documentary ENSO index from Peru, three grid cells of v wind vectors from the CLIWOC/ICOADS database, two coral records from the tropical Pacific, a SOI reconstruction based on tree rings from Indonesia and southwestern North America, a coral and tree ring based PDSI reconstruction from Java, and two Antarctic ice cores. Tables 1 and 2 show that the selected predictor series have different ending years. Therefore, there is a trade-off between maximizing the length of the overlap period with the instrumental target and minimizing the number of missing values in the predictor matrix. We find the period 1901–1995 a compromise with 5.7% (5.6%) missing values in the summer (winter) predictor matrix. Missing values in the predictor matrix of each season in this overlap period were filled in by applying an EOF (empirical orthogonal functions) based algorithm (Scherrer and Appenzeller 2006).

Table 1 Predictors used for the summer temperature reconstructions

Name	Archive	Start	End	Reference
Quelccaya accumulation	Ice core	488	2003	Thompson et al. (2000, 2006)
Quelccaya δ^{18}O	Ice core	488	2003	Thompson et al. (2000, 2006)
Laguna Aculeo pigments	Lake sediment	857	2003	von Gunten et al. (2009)
New Zealand temperature reconstruction	Tree rings	900	1999	Cook et al. (2002)
Cariaco Basin Mg/Ca	Marine sediment	1222	1990	Black et al. (2007)
Cluster CAN 11	Tree rings	1493	2002	Lara et al. (2008)
Santa Lucia	Tree rings	1646	1986	Szeicz et al. (2000)
Cluster CAN 24	Tree rings	1677	2002	Lamarche et al. (1979), Lara et al. (2008)
Cluster CAN 4	Tree rings	1704	1994	Lara et al. (2001), Schmelter (2000)
Great Barrier Reef Ba/Ca DJF	Coral	1758	1998	McCulloch et al. (2003)
Abrolhos δ^{13}C Nov/Dec	Coral	1794	1993	Kuhnert et al. (1999)
Glaciar Frias	Tree rings	1802	1985	Villalba et al. (1990)
Cluster NWA 2	Tree rings	1818	2001	Villalba et al. (1992), Morales et al. (2004)
Cluster SAN 2	Tree rings	1845	1996	Aravena et al. (2002)
Cluster CAN 16	Tree rings	1845	1994	Villalba et al. (1997a)
Cluster CAN 19	Tree rings	1865	1998	Lara et al. (2005)
Cluster CAN 14	Tree rings	1869	1994	Villalba et al. (1997a), Schmelter (2000)
Vilches	Tree rings	1880	1996	Lara et al. (2001)
Campinas DJF	Instrumental	1890	2003	Vargas and Naumann (2008)
Tucuman DJF	Instrumental	1891	2000	Vargas and Naumann (2008)
Corrientes DJF	Instrumental	1894	2004	Vargas and Naumann (2008)
Rio Gallegos DJF	Instrumental	1896	2004	Vargas and Naumann (2008)

2.3 Reconstruction methods

Three different reconstruction methodologies were applied: multivariate principal component regression (PCR), composite-plus-scaling (CPS) and regularized expectation maximization (RegEM). In PCR (Küttel et al. 2009; Luterbacher et al. 2002, 2004, 2007; Riedwyl et al. 2009; Xoplaki et al. 2005) a transfer function between a fixed number of principal components of the predictor and predictand datasets is established for the calibration period using multivariate regression based on ordinary least squares. The resulting regression models are then used to estimate the temperatures of the reconstruction period assuming temporal stability and linearity of the relation between the predictor and the predictand. A major disadvantage of regression-based reconstructions is the fact that they may be biased by a systematic loss of variance leading to underestimations of past climate variations (e.g. von Storch et al. 2004). In order to minimize such reductions of variance back in time, the temperatures reconstructed by PCR were rescaled to the mean and standard deviation of the predictand in the calibration period (e.g. Cook et al. 2004). CPS avoids this loss of variability by simply scaling a composite of the predictor data against the predictand in the calibration period (e.g. Esper et al. 2005; Jones et al. 1998). We built the composites by calculating the weighted mean of the predictors. As weighting factors, we used the correlation coefficient of each predictor with the target in the calibration period. In order to take account of the changing number of predictors over time, a variance stabilization algorithm (Frank et al. 2007) was applied to the CPS results. RegEM (Mann et al. 2007, 2008, 2009; Riedwyl et al. 2008, 2009; Rutherford et al. 2005; Schneider 2001) iteratively imputes missing values in the combined predictor–predictand input matrix until a predefined convergence criterion is fulfilled. The regression parameters between the available proxy and instrumental variables are thereby computed based on the estimated mean and covariance of the input matrix. We performed the regularization of the EM algorithm, which is necessary to avoid overfitting in the regressions, using truncated total least squares (Mann et al. 2007; Riedwyl et al. 2008, 2009). For a general comparison and description of the three approaches we refer to Jones et al. (2009) and references therein.

As the number of available predictors changes over time, the reconstructions and verifications were repeatedly performed as each predictor entered or exited the available set of proxy data (18 combinations for summer and 41 for winter) for all the three reconstruction methods.

Table 2 Predictors used for the winter temperature reconstructions

Name	Archive	Start	End	Reference
Talos deuterium	Ice core	1217	1996	Stenni et al. (2002)
Peru El Niño index	Documentary	1550	1990	García-Herrera et al. (2008), 20th century data from Quinn and Neal (1992)
Santiago de Chile precipitaion index	Documentary	1540	2006	Taulis (1934), Neukom et al. (2009)
Urvina Bay $\delta^{18}O$	Coral	1607	1981	Dunbar et al. (1994)
SOI reconstruction	Tree rings	1706	1977	Stahle et al. (1998)
Cluster SAN 4	Tree rings	1724	1984	Boninsegna et al. (1989)
Rarotonga Sr/Ca SON	Coral	1726	1996	Linsley et al. (2000)
CLIWOC/ICOADS v cell 626 JJA	Documentary/early instrumental	1750	2002	Garcia-Herrera et al. (2005), Küttel et al. (2009)
CLIWOC/ICOADS v cell 671 JJA	Documentary/early instrumental	1750	2002	Garcia-Herrera et al. (2005), Küttel et al. (2009)
CLIWOC/ICOADS v cell 672 JJA	Documentary/early instrumental	1750	2002	Garcia-Herrera et al. (2005), Küttel et al. (2009)
Monte Grande	Tree rings	1761	1988	ITRDB series arge049
Java PDSI reconstruction	Tree rings/Coral	1787	2003	D'Arrigo et al. (2006)
Law Dome 2000 $\delta^{18}O$	Ice core	1800	1999	van Ommen et al. (2004)
El Chalten Bajo	Tree rings	1807	2003	Srur et al. (2008)
Cluster ALT 1	Tree rings	1860	1993	Solíz et al. (2009)
Central Andes snow days	Documentary	1885	1996	Prieto et al. (2001a, b)
Tucuman JJA	Instrumental	1891	2000	Vargas and Naumann (2008)
Cluster CAN 17	Tree rings	1892	1994	Villalba et al. (1997a), Schmelter (2000)
Corrientes JJA	Instrumental	1894	2004	Vargas and Naumann (2008)
Rio Gallegos JJA	Instrumental	1896	2004	Vargas and Naumann (2008)

Reconstructions and statistics were then aggregated to continuous time series in such a way that every time period is reconstructed by the maximum available number of predictors. We used all three methods to perform two different reconstructions: a reconstruction optimized for the analysis of the evolution of SSA mean temperatures (henceforth SSA mean reconstruction) and a reconstruction for the analysis of spatial features, such as regional differences in trends, amplitudes and uncertainties (spatial reconstruction). The predictor and predictand datasets as well as the general reconstruction procedures used for both the SSA mean and spatial reconstructions are the same, but with slightly different methodological settings (Table 3).

We tested different truncation thresholds for the number of principal components (PCs) of the predictor data used in PCR, finally retaining the first n PCs explaining 85 (80) percent of variability in the predictor data for the SSA mean (spatial) reconstruction. This setting yielded the highest reconstruction skills (RE, r^2) for most of the evaluated predictor sets (not shown). For PCR and RegEM, the first n PCs explaining 95% of variability in the CRU TS 3 grid were used as predictand for both the SSA mean and spatial reconstructions. In the case of the SSA mean CPS reconstruction, we used the spatial average of the instrumental grid as predictand (i.e. we scaled the predictor composite to mean and standard deviation of this average series). The spatial CPS reconstruction was performed by building the composite separately for each grid cell and scaling it to the corresponding instrumental series (i.e. for each cell a separate CPS reconstruction was performed).

The quality of the instrumental grid is particularly low in some regions of SSA in the pre-1931 period, due to the sparse coverage of these areas with instrumental stations (Fig. S2, left panel; Garreaud et al. 2009). For example in Argentina, 45% of the currently available GHCN temperature station data (Peterson and Vose 1997) begin in 1931 and only 14% have data for the pre-1931 period. Nevertheless, the average over entire SSA is very likely to be reliable back to 1901, because the grid cells, which are most representative for the SSA mean, are mostly within the area with high coverage of instrumental stations back to 1901 (Fig. S2). For the SSA mean reconstructions we, therefore, used the period 1901–1995 for calibration, whereas for the spatial reconstructions, we used a shorter calibration period (1931–1995) in order to obtain reliable reconstructions in all regions (Table 3).

2.4 Reconstruction quality assessments

The uncertainties (standard errors, SE) of the Gaussian filtered reconstructions were calculated as in Xoplaki et al. (2005) by using Gaussian white noise to make the verification residuals consistent (Briffa et al. 2002; Mann et al. 1998). Uncertainties were calculated for the SSA mean, as

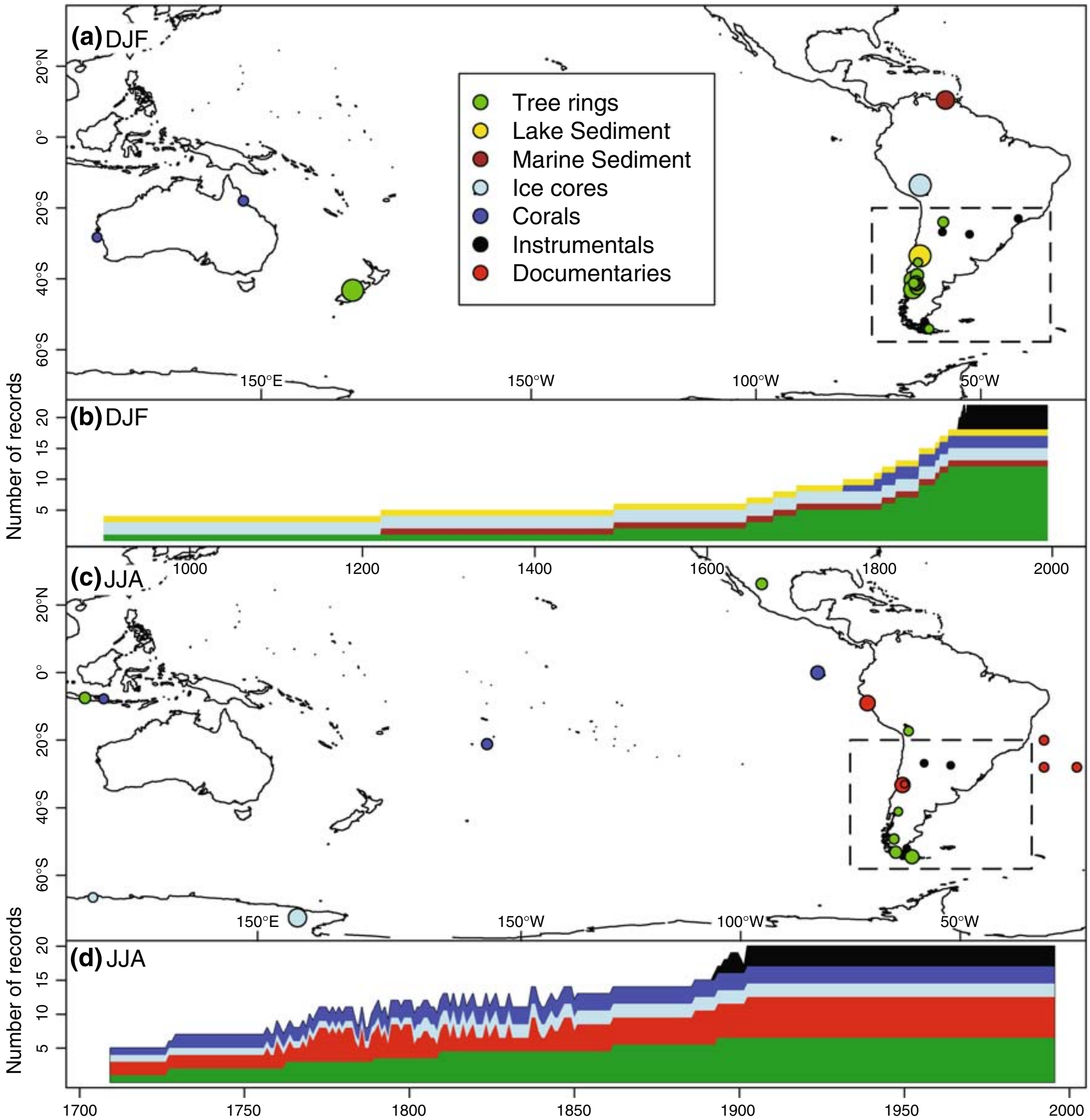

Fig. 1 Locations of the predictors used for the summer (**a**) and winter (**c**) reconstructions. The size of the *circles* represents the lengths of the series (smallest: 109 years, largest: >1,000 years). The *colors* stand for the proxy type. The reconstruction area is marked by a dashed margin. **b**, **d** Show the temporal evolution of the number of records in the final predictor set for summer and winter, respectively

well as separately for each grid cell. We used the Reduction of Error (RE, Cook et al. 1994) and r^2 values as measures of reconstruction skill. These statistics are provided as mean values of three different calibration/verification periods. We retained the first, middle and last thirds of the overlapping period for verification, respectively. Hence, for the SSA mean reconstruction we used 63 years for calibration (1901–1963, 1933–1995 and 1901–1931/1964–1995) and 32 years for verification, respectively (1964–1995, 1901–1931 and 1932–1963). Analogous statistics were computed for the spatial reconstructions between 1931 and 1995. As a further test to determine the reliability of the obtained reconstructions, we performed a second, independent reconstruction of SSA mean summer temperatures, using all the 22 summer temperature proxies (see Tables S1–S3) excluded from the optimized predictor set. For winter, the limited number of proxies (seven) that were not included into the optimized predictor matrix did not allow a skillful independent reconstruction.

3 Results

The chosen predictor network allows reconstructions of SSA summer and winter temperatures back to 900 and 1706, respectively. We focus on the PCR reconstructions in

Table 3 Overview of the settings used for the three different techniques we applied for the SSA mean (top) and spatial (bottom) temperature reconstructions

	Reconstruction technique		
	PCR	CPS	RegEM
SSA mean reconstructions			
Predictors	First *n* PCs explaining 85% of variance of optimized predictor set	Proxies of optimized predictor set with $r \geq 0.1$ with the predictand	Optimized predictor set
Predictand	First *n* PCs explaining 95% of variance of SSA CRU TS3 grid	Spatial average of CRU TS3 grid	First *n* PCs explaining 95% of variance of SSA CRU TS3 grid
Calibration period	1901–1995	1901–1995	1901–1995
Settings	OLS regression	Predictor weighting factor = *r* with the predictand	TTLS regularization; Stagn. Tol.: 10^{-4}; Truncation parameter: 3
Spatial reconstructions			
Predictors	First *n* PCs explaining 80% of variance of optimized predictor set	Proxies of optimized predictor set with $r \geq 0.1$ with the predictand	Optimized predictor set
Predictand	First *n* PCs explaining 95% of variance of SSA CRU TS3 grid	Each cell of SSA CRU TS3 grid	First *n* PCs explaining 95% of variance of SSA CRU TS3 grid
Calibration period	1931–1995	1931–1995	1931–1995
Settings	OLS regression	Predictor weighting factor = *r* with the predictand	TTLS regularization; Stagn. Tol.: 10^{-4}; Truncation parameter: 3

our results and interpretations, because they yielded the highest skill scores (see Sect. 4.3). However, the main conclusions are also valid for CPS and RegEM.

3.1 SSA mean reconstructions

The SSA mean PCR summer temperature reconstruction (top) as well as a comparison of the 30-year Gaussian filtered curves of all methods and the associated uncertainties (30-year filtered 2 SE; middle) are shown in Fig. 2 (the annual CPS and RegEM reconstructions are shown in Fig. S3). The temperatures are displayed as anomalies with respect to (wrt) the 1901–1995 calibration period. The first 350 years of the reconstruction are relatively warm, interrupted by a colder phase of about 50 years centered around 1140. At the end of the fourteenth century a relatively rapid cooling is found. The anomalously cold conditions last until the beginning of the eighteenth century. The eighteenth century is characterized by relatively warm summer temperatures. Around 1825, there is another rapid temperature decrease with a minimum in the 1850s. SSA summer temperatures thereafter steadily increase until the present. In the period 1901–1995 there is a warming trend of 0.54°C/century (0.46°C/century in the instrumental data, both with $p < 0.0001$). The reconstructed anomalies of the three likely coldest and warmest summers as well as the corresponding uncertainties are provided in Table 4 (left). The anomalies and uncertainties of the three likely coldest and warmest averages of ten consecutive summers are also shown in Table 4. The 30-year filtered 2 SE uncertainty range (Fig. 2, middle) of the PCR summer reconstruction is ±0.29°C in the year 900, ±0.26°C in 1750 and ±0.16°C in 1900. The corresponding unfiltered interannual uncertainties are ±0.87°C, ±0.79°C and ±0.53°C, respectively. In the bottom panel of Fig. 2, the standard deviations of 30-year moving windows of the temperatures reconstructed by the three methods are shown.

Figure 3 shows the annually resolved SSA mean PCR winter temperature reconstruction (top) and the comparison of the 30-year filtered reconstruction curves of the three methods (middle; annual CPS and RegEM curves see Fig. S4). Before 1930, the filtered reconstructed winter temperatures mostly remain below the average of the 1901–1995 calibration period. Short anomalously warm periods of about 10 and 15 years occur around 1815 and 1850, respectively. Also in winter, there is a warming trend in both the reconstructed (0.46°C/century, $p = 0.02$) and instrumental (0.51°C/century, $p < 0.01$) temperatures in the 1901–1995 period. The anomalies and uncertainties of the three likely coldest and warmest reconstructed years and decades are provided in Table 4 (right). The 30-year filtered (interannual) 2 SE uncertainty of the PCR reconstruction is ±0.4°C (±1.23°C) in 1706 and ±0.24°C (±0.82°C) in 1900. The bottom panel of Fig. 3 displays the 30-year moving standard deviations of the reconstructions based on the three methods.

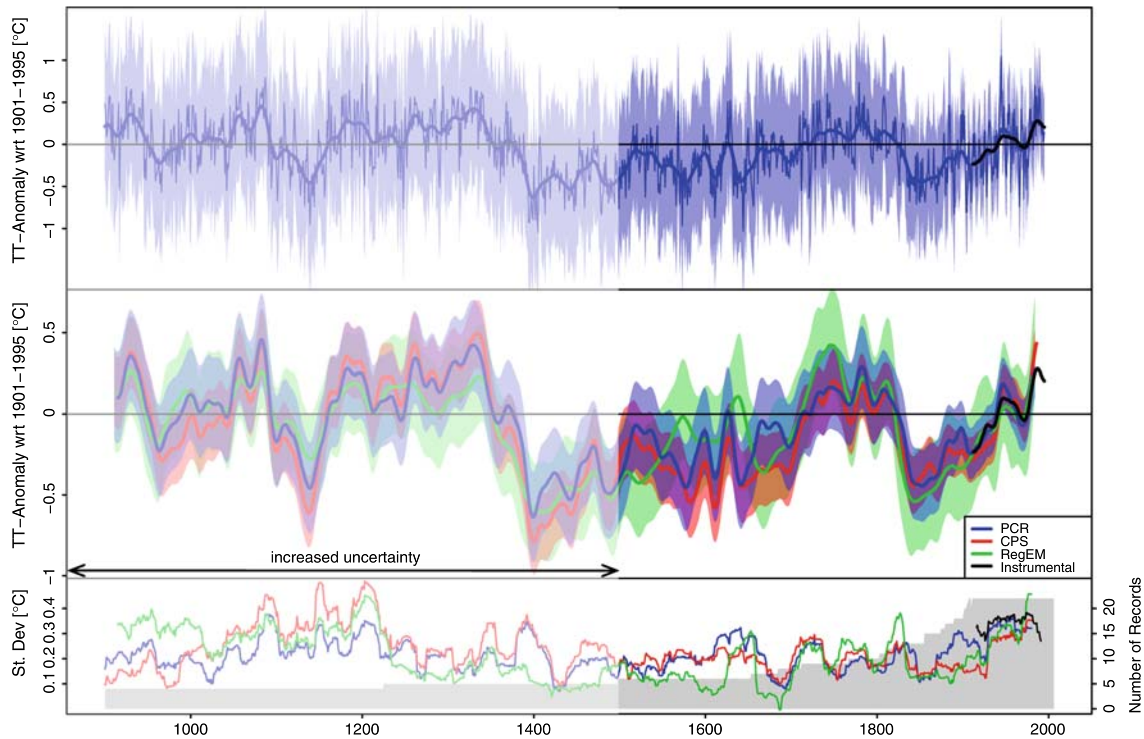

Fig. 2 *Top*: annual PCR-based reconstructed SSA mean summer (DJF) temperatures 900–1995, anomalous to the calibration period (1901–1995) mean (*blue*), and associated ±2SE uncertainty bands (*shaded*). The *thick lines* are 30-year gaussian filtered reconstructed (*blue*) and CRU gridded (*black*) temperatures. *Middle* 30-year gaussian filtered summer temperatures as in *top panel* but additionally based on CPS (*red*) and RegEM (*green*). The *black line* is again the instrumental data. The *shaded areas* represent the filtered ±2 SE uncertainty bands. *Bottom* 30-year moving standard deviations of the unfiltered reconstructions and CRU gridded data. *Shaded* is the number of predictors used for the reconstructions at each time step. The period of increased uncertainty due to the reduced predictor set (900–1492; see Sect. 4.3) is indicated by *pale colors*

Table 4 The three warmest and coldest years and (non-overlapping) decades for summer (DJF) and winter (JJA) reconstructed by PCR

	DJF		JJA	
	Years	Decades	Years	Decades
Coldest	1405 (−1.05 ± 0.86°C)	1398–1407 (−0.74 ± 0.35°C)	1870 (−1.52 ± 1.01°C)	1861–1870 (−0.83 ± 0.41°C)
2nd coldest	1644 (−1.03 ± 0.83°C)	1439–1448 (−0.73 ± 0.35°C)	1916 (−1.48 ± 0.72°C)	1823–1832 (−0.66 ± 0.45°C)
3rd coldest	1573 (−0.97 ± 0.83°C)	1485–1494 (−0.73 ± 0.35°C)	1826 (−1.39 ± 1.13°C)	1915–1924 (−0.51 ± 0.29°C)
Warmest	1945 (+1.04 ± 0.49°C)	1079–1088 (+0.57 ± 0.35°C)	1944 (+1.47 ± 0.72°C)	1939–1948 (+0.55 ± 0.29°C)
2nd warmest	1205 (+0.95 ± 0.87°C)	1325–1334 (+0.49 ± 0.35°C)	1855 (+1.32 ± 1.14°C)	1810–1819 (+0.45 ± 0.46°C)
3rd warmest	1218 (+0.83 ± 0.87°C)	925–934 (+0.44 ± 0.35°C)	1761 (+1.13 ± 1.2°C)	1850–1859 (+0.34 ± 0.44°C)

The corresponding anomalies with respect to the period 1901–1995 and uncertainties are indicated in parentheses

3.2 Spatial SSA reconstructions

To identify regional differences in the spatial reconstructions, we defined the following four sub-regions (Fig. S5): South Patagonia (SP; all grid cells south of 45°S); North Patagonia (NP, 37°S–45°S), the Central Chile (CC, 27°S–42°S, along the Pacific coast, average latitudinal extent of four grid boxes) and the remaining areas in subtropical SSA (ST). The 30-year filtered mean summer temperature anomalies of the four regions, reconstructed by PCR (spatial reconstructions), are displayed in Fig. 4. It shows that in summer, the decadal-scale variability is largest in CC, followed by SP and NP. In the ST region, the variability is clearly reduced, as compared to the other regions. These differences in variability between the regions are also visible in the instrumental data, albeit the reduction of variability in ST is smaller (Table S4). Before ca. 1650, the temperatures generally fluctuate synchronously in all

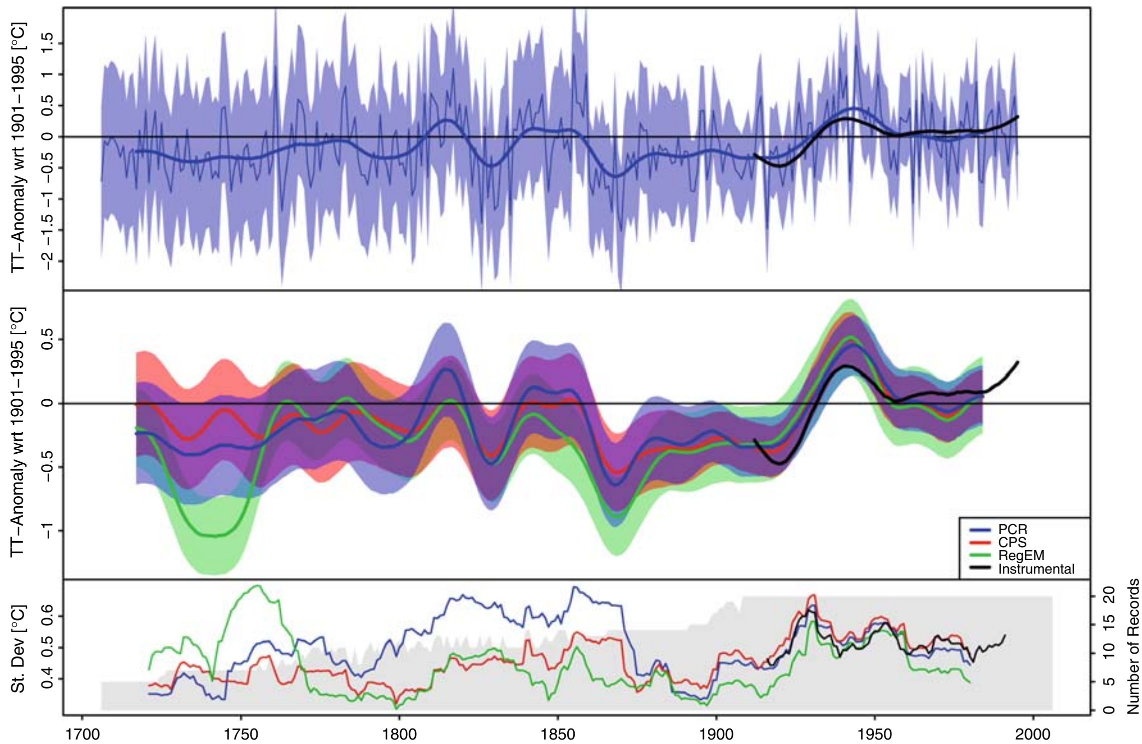

Fig. 3 Same as Fig. 2 but for winter (JJA) and the period 1706–2006. Notice the different scale of the *y* axes

regions, but with different magnitudes (Fig. 4). Afterwards, the temperature fluctuations of the sub-regions are more variable at the decadal scale, however still synchronous on multi-decadal to centennial scales (e.g. the warm eighteenth and cold nineteenth centuries). The first (second) panel of Fig. 5 displays the mean temperature anomalies of the summers 1846–1875 (1775–1804), being the coldest (warmest) consecutive 30 years of the pre-1901 period (−0.64 ± 0.34°C and +0.22 ± 0.39°C, respectively). In both cases, the temperature pattern is spatially uniform over most of the continent, with some areas in the north showing different sign. The difference between the two periods (warm–cold) is displayed in the third panel of Fig. 5. The largest values correspond to central Patagonia (i.e. the highest amplitude on 30-year timescales in the pre-1901 period), while the smallest difference is found in the northernmost areas of SSA. The filtered 2 SE values expressed in °C, averaged over the 900–1995 period are shown in the right panel of Fig. 5. The uncertainties are largest in northwestern Argentina and in central Patagonia.

Figure 6 shows the 30-year filtered winter reconstructions of the sub-regions. The differences between the regions are more pronounced than in summer, especially for SP and after 1800. Figure 7 (first two panels) shows average anomalies of the years 1727–1756 (1794–1823), the coldest (warmest) 30 consecutive winters of the 1706–1900 period (−1.09 ± 0.75°C and −0.56 ± 0.65°C, respectively). The amplitudes (Fig. 7 third panel) are largest in central-northern SSA and smallest in northeastern SSA. The average 30-year filtered SE values 1706–1995 are displayed in the right panel of Fig. 7. The areas with large uncertainties are more widespread in winter (Fig. 7) than in summer (Fig. 5) and cover large parts of SSA east of the Andes.

3.3 Quality assessments

The correlations of the PCR SSA mean reconstructions with the instrumental data in the 1901–1995 period are 0.89 for summer and 0.71 for winter (both $p < 0.001$). The evolution of the RE and r^2 values of the SSA mean PCR reconstructions over time as well as the percentage of grid cells with positive REs in the spatial PCR reconstructions are shown in Fig. 8 (corresponding curves for CPS and RegEM, Figs. S6 and S7). The general evolution of the RE and r^2 values is similar for summer and winter. In the first years of the summer (winter) reconstruction the RE values are very close to zero and remain between 0.2 and 0.4 after 1222 (1787). They reach maximum values of 0.73 (summer) and 0.66 (winter) at the end of the nineteenth century, respectively, where instrumental temperature series become increasingly available (Tables 1, 2). The percentage of grid cells with positive REs in the spatial PCR reconstructions (i.e. with higher skill than climatology) is

Fig. 4 30-year filtered summer temperature anomalies 900–1995 (wrt 1901–1995) for different sub-regions of SSA (see Fig. S5) reconstructed by PCR

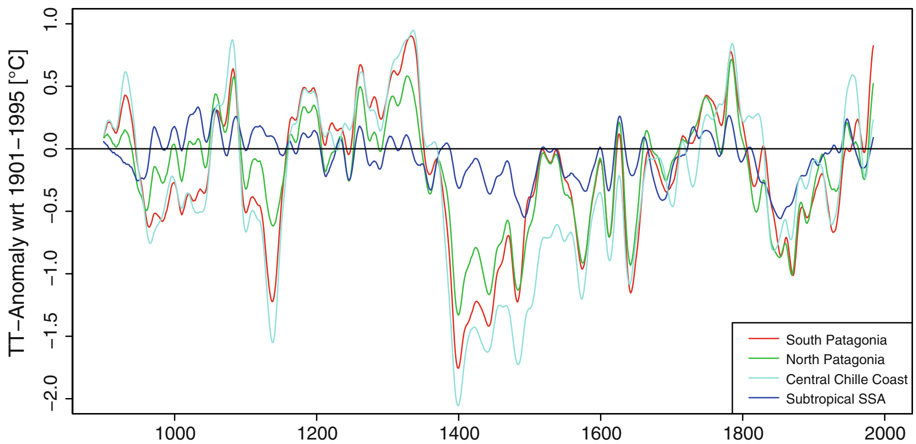

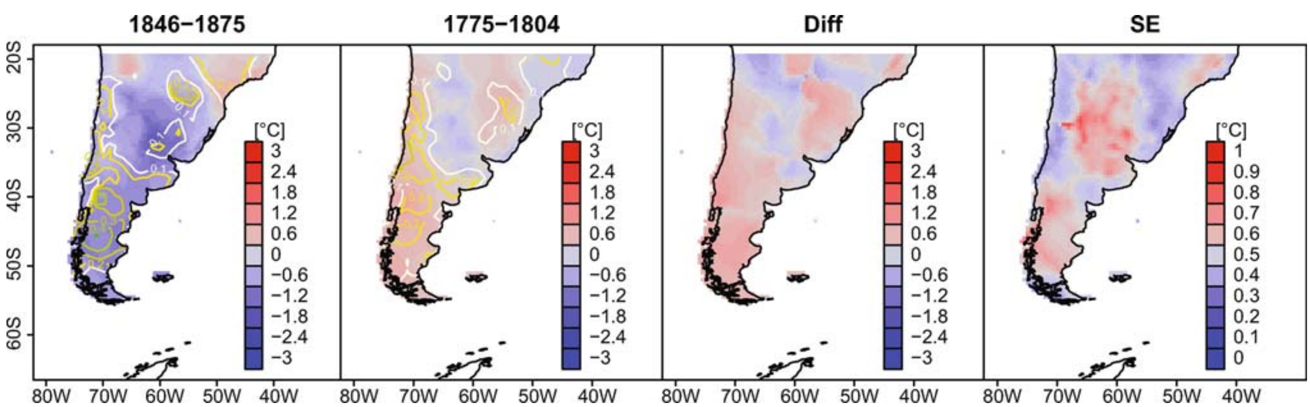

Fig. 5 *First (second) panel* average temperature anomalies 1846–1875 (1775–1804), the coldest (warmest) 30 consecutive years of the spatial PCR summer reconstruction. Average REs over the period are indicated by *contour lines*. *Third panel* difference between the means of these two periods (warm minus cold). *Last panel* Mean 30-year filtered uncertainties in the PCR reconstruction (900–1995)

relatively stable over time in summer (between 60 and 75%; Fig. 8, red lines). They are clearly lower in winter, starting at 50% in the early eighteenth century but increasing to 87% at the end of the reconstruction period. In summer, the lowest RE values are found in the central-northern and southernmost parts of SSA; the highest values are located around 45°S and in central Chile (contour lines in Fig. 5). In winter, the area with the lowest REs is central SSA east of the Andes; the regions with the highest skill are central and northern Chile (contour lines in Fig. 7). As indicated in Figs. 5 and 7, the spatial distribution of the REs remains rather stable over time.

Figure 9a shows the 30-year Gaussian filtered SSA mean summer PCR reconstruction (blue) along with the independent PCR reconstruction based on the 22 withheld summer predictors (green). Due to the limited number of available predictors, the reconstruction based on the withheld predictors yielded skillful results (RE > 0) only back to 1232. Although the amplitudes of the two curves differ, the temporal evolutions of the two reconstructions are similar on centennial timescales. The red curve in Fig. 9a shows the reconstruction obtained when only using those proxies of the optimal set which are from within SSA. It covers the period 1677 (four SSA predictors available) to 1995. The decadal scale variations are very similar to the original reconstruction and the correlations between the two reconstructions are 0.82 on interannual and 0.95 on 30-year timescales (both $p < 0.001$). Also in winter, the reconstruction based only on proxies from within SSA (covering 1807, where four proxies are available, to 1995) is very similar to that based on the optimized predictor set (Fig. 9b). Here, the correlations are 0.81 (interannual) and 0.92 (30 year-filtered; both $p < 0.001$).

As a further validation, we compared our results with the annual temperature reconstructions of the NP and SP Andes (Villalba et al. 2003) based on tree ring records independent from our reconstructions. For comparison, we constructed annual mean values of our results by averaging the reconstructed summer and winter anomalies. The 30-year filtered anomalies of both reconstructions are shown in Figs. 9c (NP) and d (SP). The correlations between our SP (NP) annual reconstructions and the results of Villalba

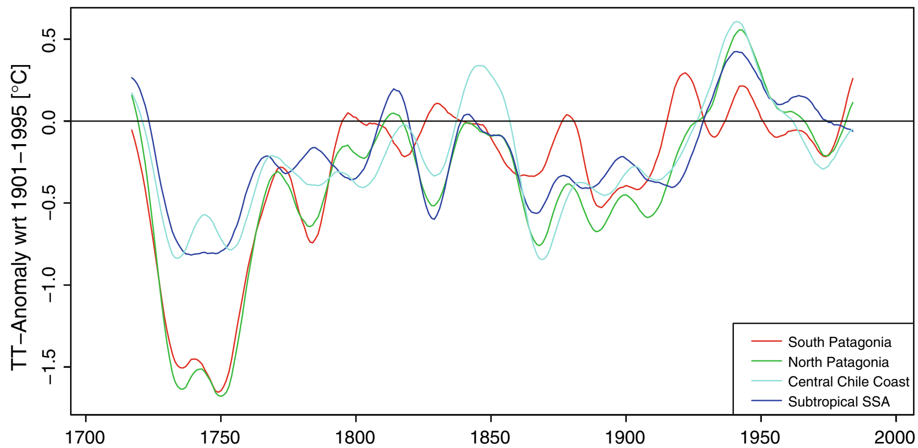

Fig. 6 Same as Fig. 4 but for winter and the period 1706–1995. Notice the different scale of the *y*-axis

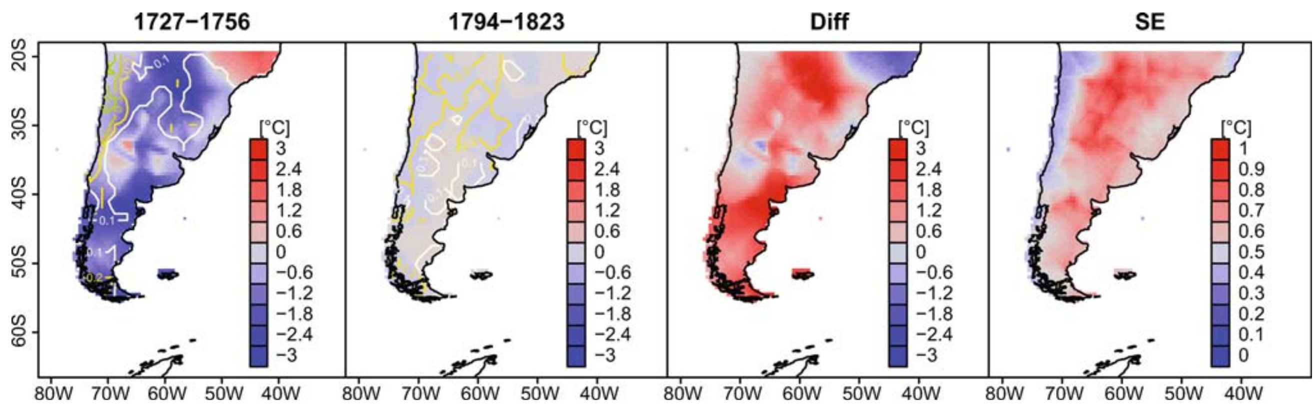

Fig. 7 Same as Fig. 5 but for winter and the coldest (warmest) period 1727–1756 (1794–1823)

et al. (2003) are 0.28 (0.31) for the unfiltered and 0.37 (0.71) for the 30-year filtered data and are significant ($p < 0.001$). However, our results do not depict the strong negative anomalies in the seventeenth and eighteenth centuries found in SP by Villalba et al. (2003; Fig. 9d).

Finally, we calculated the correlations of long (non-homogenized) instrumental temperature records with the spatial reconstructions at the corresponding grid cells (Table 5). As long records, we defined stations with available data for at least 30 years in both the calibration (1931–1995) and reconstruction (pre-1931) periods (sources: GHCN; Peterson and Vose 1997 and Servicio Meteorologico Nacional de Argentina, personnal communication 2008). Significant correlations ($p < 0.01$) are marked with an asterisk (Table 5). Most stations have significant but not very high correlations ($r = 0.55$ on average). Most of the station data with non-significant correlations have either non-significant correlations also in the calibration period (1931–1995) or do not correlate significantly with the corresponding predictand grid cell in the verification period. Non-significant correlations mainly occur at stations in southern Patagonia or in the northeastern part of SSA.

4 Discussion

4.1 SSA mean reconstructions

Our summer temperature reconstructions (Fig. 2) suggest that a warm period extended in SSA from 900 (or even earlier) to the mid-fourteenth century. This is towards the end of the Medieval Climate Anomaly (MCA; Bradley et al. 2003; Stine 1994) as concluded from NH temperature reconstructions, where most studies find a termination between ca. 1200–1350 (Jansen et al. 2007; Wanner et al. 2008). Major advances of several summer temperature sensitive glaciers from the eastern slopes of the Patagonian Andes occurred in the seventeenth century and between 1850 and 1950 (Koch and Kilian 2005; Luckman and Villalba 2001), coinciding with periods of low temperatures in our reconstruction (Fig. 2). However, the reconstructed cold period in the early fifteenth century corresponds only for a few SSA glaciers with a period of advance (e.g. Glaciar Huemul, Masiokas et al. 2009; Röthlisberger 1986). This may be due to the still limited knowledge about glacial fluctuations in the area and their

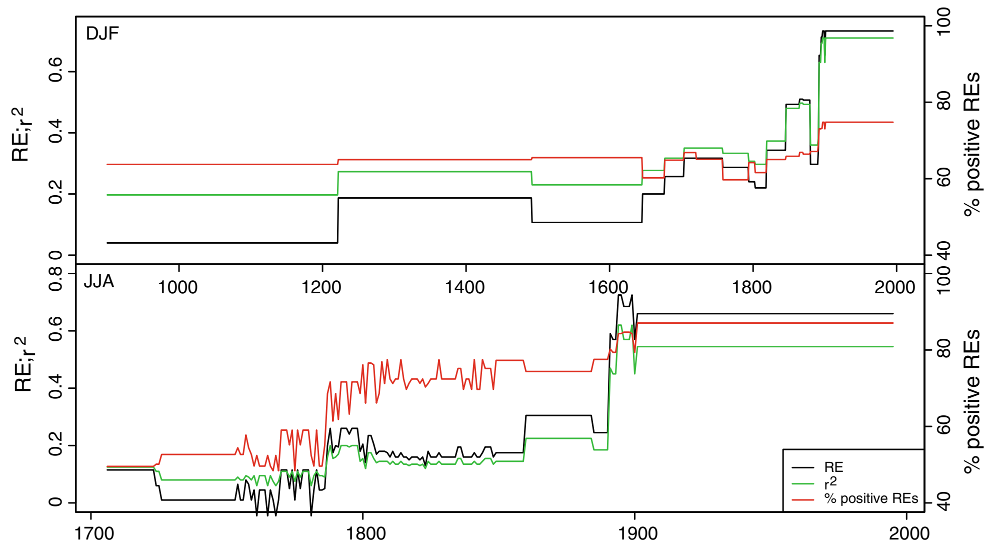

Fig. 8 Skill measures of the PCR reconstructions. RE (*black*) and r^2 (*green*) of the SSA mean reconstructions as well as the fraction of grid cells with positive RE values of the spatial reconstructions (*red*). *Top* summer 900–1995. *Bottom* winter 1706–1995. The values represent averages of three calibration/verification intervals (see text for details)

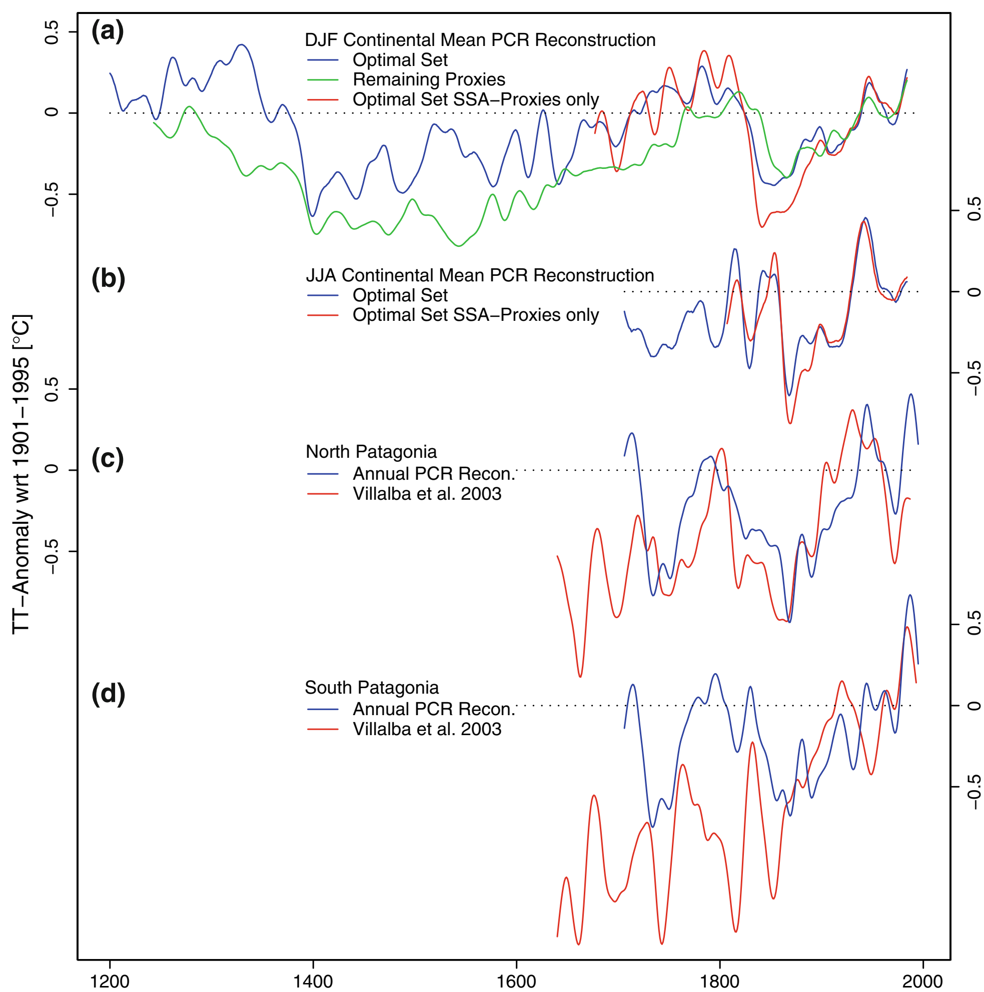

Fig. 9 **a** 30-year filtered SSA mean summer temperatures reconstructed by PCR using all proxies of the optimized predictor set (*blue*; 1200–1995), the withheld summer temperature predictors (*green*; 1232–1995) and only the proxies of the optimized set that are situated within SSA (*red*; 1677–1995). **b** 30-year filtered SSA mean winter temperatures reconstructed by PCR using all proxies of the optimized predictor set (*blue*; 1706–1995) and only the proxies of the optimized set that are situated within SSA (*red*; 1807–1995). 30-year filtered reconstructed annual (average of DJF and JJA) anomalies (*blue*; 1706–1995) for North Patagonia (**c**) and South Patagonia (**d**) compared to the independent reconstructions of Villalba et al. (2003; *red*; 1640–1995)

relationship to climate (Koch and Kilian 2005; Luckman and Villalba 2001; Masiokas et al. 2009) or due to the lack of proxy information from southern SSA before 1493 in our reconstruction (Table 1). Interestingly, the dates of glacial advances in New Zealand around 1000, 1150, 1400, 1600, 1700 and in the nineteenth century (Schaefer et al.

Table 5 Long instrumental temperature stations used for verification

Station name	Start	End	Lat S	Lon W	cor DJF	cor JJA
Ushuaia	1901	1986	54.8	68.32	0.38[a]	0.63*
Punta Arenas	1888	1991	53	70.85	0.08[b]	0.34
Santa Cruz Aero	1901	1989	50.02	68.57	0.28[a]	0.71*
Trelew Aero	1901	1989	43.2	65.27	0.51*	0.3[a]
Esquel	1901	1983	42.97	71.15	0.49*	0.07[b]
Bahia Blanca Aero	1860	1989	38.7	62.2	0.41*	0.32
Prado	1883	1988	34.85	56.2	0.67*	0.69*
Buenos Aires	1856	1989	34.58	58.48	0.57*	0.43*
Pudahuel	1861	2008	33.38	70.78	0.35*	0.65*
San Juan	1901	1985	31.57	68.87	0.77*	0.52*
Cordoba	1873	1986	31.4	64.2	0.69*	0.4*
Punta Tortuga	1901	1980	29.9	71.4	0.51*	0.66*
Goya	1877	1960	29.1	59.3	0.59*	0.73*
Curitiba	1885	1991	25.43	49.27	0.5*	0.53*
Asuncion Aero	1893	1990	25.27	57.63	0.39	0.71*
Salta Aero	1901	1989	24.85	65.48	0.81*	0.65*
Iguape	1895	1987	24.72	47.55	0.2[a]	0.19
Sao Paolo	1887	1991	23.5	46.62	0.4*	0.33[a]
Rio de Janeiro	1871	1990	22.92	43.17	0.38*	0.38*

Station names, beginning and end years of the measurements and coordinates. Correlations with the spatial summer and winter PCR reconstructions at the corresponding grid cells in the pre-1931 overlap periods

[a] Correlation of station data with the predictand is not significant in the verification period

[b] Correlation is not significant also in the calibration period

* Significant correlations ($p < 0.01$)

2009) mostly coincide with cold periods in our SSA summer temperature reconstructions. This is also confirmed if the proxy record from New Zealand is removed from the predictor set (Fig. S8). This suggests that the teleconnections between the SSA and New Zealand areas as found in the instrumental record (e.g. Villalba et al. 1997b) were persistent over the last millennium. The warm temperatures reconstructed in the twentieth century are of similar amplitude as in preceding warm periods within the last millennium (Fig. 2).

4.2 Spatial reconstructions

The temperature variations of the different sub-regions of SSA are broadly synchronous at multi-decadal to centennial scales, albeit with different amplitudes (Figs. 4, 6). At annual to decadal timescales (except for the pre-1650 period in summer), the temperatures of the sub-regions exhibit more individual fluctuations (Figs. 4, 5, 6, 7 and S9, S10), but remain mostly within the 2 SE uncertainty bands of each individual region (not shown). The strong synchronicity in summer temperatures before 1650 might be an artifact caused by the decreasing number of available predictors back in time leading to reduced spatial variability and more fitting towards mean conditions. As also found in regional reconstructions from the NH and the tropics (Jansen et al. 2007; Rabatel et al. 2008; Wanner et al. 2008), the timing and extent of the warmest and coolest periods in our reconstructions vary in different parts of SSA (Fig. 4): The warm peaks between 900 and 1350 are distinct in SP, NP and CC with 30-year filtered anomalies of up to +0.9°C (wrt 1901–1995, Fig. 4) in the late thirteenth and early fourteenth centuries. In these regions, the transition to colder conditions is characterized by two rapid temperature decreases between 1335 and 1355 as well as between 1370 and 1400. The reconstructions of the ST region can be clearly distinguished from the other regions due to the weak warm anomalies before 1350, the absence of the distinct cool period at the beginning of the fifteenth century and the pronounced minimum around 1850 in summer (Fig. 4). The distinct differences in variability between the sub-regions may also be an artifact of the strong limitations of the instrumental target in broad regions of SSA due to the sparse coverage with station data (Garreaud et al. 2009; see also Fig. S2).

4.3 Quality considerations

The three methodologies used herein (PCR, CPS and RegEM) lead to comparable reconstructions at decadal to centennial timescales (Figs. 2, 3, middle panels and Figs. S3, S4, S6, S7, S11, S12). Particularly the results of PCR and CPS are remarkably similar, with a slightly different temperature history estimated by RegEM (Figs. 2, 3). The bottom panels of Figs. 2 and 3 suggest that none of the applied methods systematically over- or under-estimates the interannual variance back in time. We mainly base our discussions on the results of PCR, because this method yielded the highest skill scores (Figs. S6, S7). The PCR and CPS reconstructions are relatively robust to changes in reconstruction parameters, calibration period (see Figs. S13, S14) or predictor subset (see Figs. 9, S11). In contrast, the results of the RegEM reconstructions are sensitive to changes in the truncation parameter, predictor set and calibration period chosen; particularly in the spatial reconstructions with short calibration periods (see e.g., Fig. S11). The summer temperature reconstruction, which we performed based on a completely independent predictor set (see Sect. 3.3), has a qualitatively similar pattern at centennial timescales (Fig. 9). Also, the reconstructions based only on predictors from within SSA are very similar to the results of our optimized sets in both seasons (Fig. 9), indicating that including proxies from areas outside SSA does not lead to biases in our reconstructions, at least as regards the SSA mean. Moreover, our reconstructions are not dominated by single proxies, as shown by the individual regression weights of each proxy in PCR (Figs. S15–S18). We therefore argue that the reconstructed low frequency patterns are relatively robust with respect to the reconstruction methodology and predictor set used.

Our results suggest that the selected predictors are able to capture regional differences in past SSA temperatures at interannual (illustrated by Figs. S9, S10) and decadal timescales (Figs. 4, 5, 6, 7, 9). This finding is corroborated by the significant correlations with the independent regional reconstructions of the southern Andes (Villalba et al. 2003) and the long temperature measurements from SSA (Table 5). However, most of these correlations are significant though rather low, indicating that our reconstructions have limited potential for local to regional analyses in the complex mountain areas of the Andes and in the peripheral regions of SSA.

The reconstruction uncertainties are smaller in summer than in winter (Figs. 2, 3, 5, 7, S9 and S10), indicating that the quality of the predictor network is higher in summer. Generally, our reconstructions and verification exercises yielded mostly positive but relatively low skill scores for both seasons (Figs. 5, 7, 8). It must be noted that we optimized our predictor set based on these skill scores which are, therefore, very probably overestimated to a certain extent. The lowest skill and the largest uncertainties (Figs. 5, 7) correspond mostly to the lowlands east of the Andes, from where no annually resolved temperature proxies are available (Fig. 1). We emphasize that in the period before 1493, the summer temperature reconstructions exhibit larger uncertainties (as illustrated in Fig. 2), because all but one predictor used in this timeframe stem from outside SSA and are only connected to its climate through teleconnections which are assumed to remain stable over time. However, Fig. S8 shows that the record from within SSA has the largest influence on the reconstruction in this period (900–1492). Furthermore, a reconstruction based only on SSA proxies (some of them not included in the optimal set) reveals similar results. This indicates that the reconstructions reflect realistic fluctuations of SSA temperatures, also in this early period (details see supplementary material). The results are generally more uncertain in winter than in summer, because in winter, the relation to SSA winter temperature is found by correlation analysis only and has not been explicitly stated in literature for most of the non-instrumental proxies used. The only exception are the tree ring records from South Patagonia and Tierra del Fuego, which Aravena et al. (2002) found to be related to annual minimum temperatures. These findings underline the need for more highly resolved temperature proxies from within SSA, particularly in other seasons than summer and in the eastern part of the continent.

5 Conclusions and outlook

Twenty two (20) carefully selected proxies were used to statistically reconstruct austral summer (winter) temperatures of SSA back to 900 (1706) using PCR, CPS and RegEM. The results represent the first seasonal sub-continental-scale climate field reconstructions of the SH going so far back in time. The reconstructed SSA mean summer temperatures are characterized by warm episodes before 1350, between 1710 and 1820 and after 1940. Cold conditions prevailed between 1400 and 1650 as well as between 1820 and 1940. This mostly agrees with reconstructions of fluctuations of temperature sensitive glaciers in SSA and New Zealand. In winter, the decadal-scale pre-1901 temperature anomalies mostly remain below the twentieth century average. Within the twentieth century, the 30-year filtered anomalies of both seasons do not exceed the uncertainty range of warm periods in previous centuries. Our spatial reconstructions indicate differences in the low and high frequency variability between the sub-regions of SSA. This study clearly revealed that temporally and spatially highly resolved multi-centennial climate field reconstructions are also possible in the SH. Nevertheless, skill values are still rather low and there is a striking lack of annually resolved proxy data, especially from tropical and subtropical regions (see Boninsegna et al. 2009) and from the eastern lowlands of SSA.

Together with reconstructions from other regions, our reconstructions allow quantification of differences and similarities of past temperature variations of different continents and hemispheres and to put the recent warming into a larger temporal and spatial context (as intended by the PAGES 2k initiative; Newman et al. 2009). Besides, they can serve as a basis for the analysis of environmental and societal changes of the last millennium in SSA as well as for comparison and calibration issues of proxies with lower resolution. Along with forthcoming reconstructions of precipitation (Neukom et al. 2010) and sea level pressure, our results will help to understand the influence of globally relevant large scale patterns, such as ENSO, SAM and PDO on the climate of SSA as well as regional expressions of solar and volcanic forcings. Finally, the reconstructions can be used for comparison with the outputs of global climate model (GCM) simulations (Meyer and Wagner 2008a, b. Such comparisons can help to improve the understanding of the processes driving past climate variability in SSA and also to assess and ultimately improve the ability of GCMs to simulate past and future climate variability.

Acknowledgments RN is supported by the by the Swiss NSF through the NCCR Climate. JL acknowledges support from the EU/FP7 project ACQWA (grant 212250). We thank the Servicio

Meteorologico Nacional de Argentina and Gustavo Naumann for kindly providing the station data. We also thank Jan Esper and Ulf Büntgen for support in the development of the tree ring chronologies. Many thanks go to all contributors of proxy data and to PAGES for supporting the initiative LOTRED South America. The reviewers made useful comments and suggestions and helped to improve the quality of this study.

References

Aravena JC, Lara A, Wolodarsky-Franke A, Villalba R, Cuq E (2002) Tree-ring growth patterns and temperature reconstruction from *Nothofagus pumilio* (Fagaceae) forests at the upper tree line of southern Chilean Patagonia. Revista Chilena De Historia Natural 75:361–376

Black DE, Abahazi MA, Thunell RC, Kaplan A, Tappa EJ, Peterson LC (2007) An 8-century tropical Atlantic SST record from the Cariaco Basin: Baseline variability, twentieth-century warming, and Atlantic hurricane frequency. Paleoceanography 22: PA4204

Boninsegna JA, Keegan J, Jacoby GC, D'Arrigo R, Holmes RL (1989) Dendrochronological studies in Tierra del Fuego, Argentina. Quat South Am 7:315–326

Boninsegna JA et al (2009) Dendroclimatological reconstructions in South America: a review. Palaeogeogr Palaeoclimatol Palaeoecol 281:210–228

Bradley RS, Hughes MK, Diaz HF (2003) Climate in Medieval time. Science 302:404–405

Briffa KR, Osborn TJ, Schweingruber FH, Jones PD, Shiyatov SG, Vaganov EA (2002) Tree-ring width and density data around the Northern Hemisphere: Part 1, local and regional climate signals. Holocene 12:737–757

Brohan P, Kennedy JJ, Harris I, Tett SFB, Jones PD (2006) Uncertainty estimates in regional and global observed temperature changes: a new data set from 1850. J Geophys Res Atmos. 111: 21 p

Busalacchi AJ (2004) The role of the Southern Ocean in global processes: an earth system science approach. Antarct Sci 16:363–368

Cook ER, Briffa KR, Jones PD (1994) Spatial regression methods in dendroclimatology—a review and comparison of 2 techniques. Int J Climatol 14:379–402

Cook ER, Palmer JG, D'Arrigo RD (2002) Evidence for a 'Medieval Warm Period' in a 1, 100 year tree-ring reconstruction of past austral summer temperatures in New Zealand. Geophys Res Lett 29:1667

Cook ER, Woodhouse CA, Eakin CM, Meko DM, Stahle DW (2004) Long-term aridity changes in the western United States. Science 306:1015–1018

D'Arrigo R et al (2006) Monsoon drought over Java, Indonesia, during the past two centuries. Geophys Res Lett 33:L04709

Dettinger MD, Battisti DS, Garreaud RD, McCabe GJ, Bitz CM (2001) Interhemispheric effects of interannual and decadal ENSO-like climate variations on the Americas. In: Markgraf V (ed) Interhemispheric climate linkages. Cambridge University Press, Cambridge, pp 1–16

Dunbar RB, Wellington GM, Colgan MW, Glynn PW (1994) Eastern Pacific sea-surface temperature since 1600-AD—the delta-O-18 record of climate variability in Galapagos corals. Paleoceanography 9:291–315

Esper J, Frank DC, Wilson RJS, Briffa KR (2005) Effect of scaling and regression on reconstructed temperature amplitude for the past millennium. Geophys Res Lett 32:L07711

Frank D, Esper J, Cook ER (2007) Adjustment for proxy number and coherence in a large-scale temperature reconstruction. Geophys Res Lett 34:L16709

García-Herrera R, Konnen GP, Wheeler DA, Prieto MR, Jones PD, Koek FB (2005) CLIWOC: A climatological database for the world's oceans 1750–1854. Clim Change 73:1–12

García-Herrera R et al (2008) A chronology of El Niño events from primary documentary sources in northern Peru. J Clim 21:1948–1962

Garreaud RD, Battisti DS (1999) Interannual (ENSO) and interdecadal (ENSO-like) variability in the Southern Hemisphere tropospheric circulation. J Clim 12:2113–2123

Garreaud RD, Vuille M, Compagnucci R, Marengo J (2009) Present-day South American climate. Palaeogeogr Palaeoclimatol Palaeoecol 281:180–195

Jansen E et al (2007) Palaeoclimate, in Climate Change 2007: the physical science basis. In: Solomon S et al (ed) Contribution of working group I to the fourth assessment report of the intergovernmental panel on climate change. Cambridge, United Kingdom and New York, NY, USA

Jones PD, Briffa KR, Barnett TP, Tett SFB (1998) High-resolution palaeoclimatic records for the last millennium: interpretation, integration and comparison with General Circulation Model control-run temperatures. Holocene 8:455–471

Jones PD et al (2009) High-resolution palaeoclimatology of the last millennium: a review of current status and future prospects. Holocene 19:3–49

Koch J, Kilian R (2005) 'Little Ice Age' glacier fluctuations, Gran Campo Nevado, southernmost Chile. Holocene 15:20–28

Kuhnert H et al (1999) A 200-year coral stable oxygen isotope record from a high-latitude reef off western Australia. Coral Reefs 18:1–12

Küttel M, Luterbacher J, Zorita E, Xoplaki E, Riedwyl N, Wanner H (2007) Testing a European winter surface temperature reconstruction in a surrogate climate. Geophys Res Lett 34:L07710

Küttel M et al (2009) The importance of ship log data: reconstructing North Atlantic, European and Mediterranean sea level pressure fields back to 1750. Clim Dyn. doi:10.1007/s00382-00009-00577-00389

Lamarche VC, Holmes RL, Dunwiddie PW, Drew LG (1979) Tree-ring chronologies of the southern hemisphere: vol 1: Argentina. Chronology Series V, Laboratory of Tree-Ring Research. University of Arizona, Tucson

Lara A, Villalba R (1993) A 3620-year temperature record from Fitzroya-Cupressoides tree rings in Southern South-America. Science 260:1104–1106

Lara A, Aravena JC, Villalba R, Wolodarsky-Franke A, Luckman B, Wilson R (2001) Dendroclimatology of high-elevation Nothofagus pumilio forests at their northern distribution limit in the central Andes of Chile. Can J Forest Res 31:925–936

Lara A, Villalba R, Wolodarsky-Franke A, Aravena JC, Luckman BH, Cuq E (2005) Spatial and temporal variation in Nothofagus pumilio growth at tree line along its latitudinal range (35 degrees 40 '-55 degrees S) in the Chilean Andes. J Biogeogr 32:879–893

Lara A, Villalba R, Urrutia R (2008) A 400-year tree-ring record of the Puelo River summer-fall streamflow in the Valdivian Rainforest eco-region, Chile. Clim Change 86:331–356

Linsley BK, Wellington GM, Schrag DP (2000) Decadal sea surface temperature variability in the subtropical South Pacific from 1726 to 1997 AD. Science 290:1145–1148

Ljungqvist FC (2009) Temperature Proxy Records covering the last two Millennia: a tabular and visual Overview. Geografiska Annaler: Ser A, Phys Geogr 91:11–29

Luckman B, Villalba R (2001) Assessing the synchronicity of glacier fluctuations in the western Cordillera of the Americas during the last millennium. In: Markgraf V (ed) Inter-hemispheric climate linkages. Academic Press, San Diego, pp 119–140

Luterbacher J et al (2002) Reconstruction of sea level pressure fields over the Eastern North Atlantic and Europe back to 1500. Clim Dyn 18:545–561

Luterbacher J, Dietrich D, Xoplaki E, Grosjean M, Wanner H (2004) European seasonal and annual temperature variability, trends, and extremes since 1500. Science 303:1499–1503

Luterbacher J, Liniger MA, Menzel A, Estrella N, Della-Marta PM, Pfister C, Rutishauser T, Xoplaki E (2007) The exceptional European warmth of autumn 2006 and winter 2007: historical context, the underlying dynamics and its phenological impacts. Geophys Res Lett 34:L12704

Mann ME, Jones PD (2003) Global surface temperatures over the past two millennia. Geophys Res Lett 30:1820

Mann ME, Bradley RS, Hughes MK (1998) Global-scale temperature patterns and climate forcing over the past six centuries. Nature 392:779–787

Mann ME, Rutherford S, Wahl E, Ammann C (2007) Robustness of proxy-based climate field reconstruction methods. J Geophys Res 112:D12109

Mann ME, Zhang ZH, Hughes MK, Bradley RS, Miller SK, Rutherford S, Ni FB (2008) Proxy-based reconstructions of hemispheric and global surface temperature variations over the past two millennia. Proc Natl Acad Sci USA 105:13252–13257

Mann ME et al (2009) Global signatures and dynamical origins of the little ice age and medieval climate anomaly. Science 326:1256–1260

Masiokas MH, Luckman BH, Villalba R, Delgado S, Skvarca P, Ripalta A (2009) Little Ice Age fluctuations of small glaciers in the Monte Fitz Roy and Lago del Desierto areas, south Patagonian Andes, Argentina. Palaeogeogr Palaeoclimatol Palaeoecol 281:351–362

McCulloch M, Fallon S, Wyndham T, Hendy E, Lough J, Barnes D (2003) Coral record of increased sediment flux to the inner Great Barrier Reef since European settlement. Nature 421:727–730

Meyer I, Wagner S (2008a) The Little Ice Age in southern South America: proxy and model based evidence. In: Vimeux F et al (eds) Past climate variability in South America and surrounding regions from the last glacial maximum to the Holocene, pp 395–412. doi:10.1007/978-90-481-2672-9

Meyer I, Wagner S (2008b) The Little Ice Age in southern Patagonia-comparison between paleo-ecological reconstructions and downscaled model output of a GCM simulation. PAGES News 16(2):12–13

Mitchell TD, Jones PD (2005) An improved method of constructing a database of monthly climate observations and associated high-resolution grids. Int J Climatol 25:693–712

Morales MS, Villalba R, Grau HR, Paolini L (2004) Rainfall-controlled tree growth in high-elevation subtropical treelines. Ecology 85:3080–3089

Neukom R et al (2009) An extended network of documentary data from South America and its potential for quantitative precipitation reconstructions back to the 16th century. Geophys Res Lett 36:L12703

Neukom R et al (2010) Multi-centennial summer and winter precipitation variability in southern South America. Geophys Res Lett (revised)

Newman L, Wanner H, Kiefer T (2009) Towards a global synthesis of the climate of the last two millennia. PAGES news 17:130–131

Peterson TC, Vose RS (1997) An overview of the global historical climatology network temperature database. Bull Am Meteorol Soc 78:2837–2849

Prieto MDR, García Herrera R (2009) Documentary sources from South America: Potential for climate reconstruction. Palaeogeogr Palaeoclimatol Palaeoecol 281:196–209

Prieto MR, Herrera R, Castrillejo T, Dussel P (2001a) Variaciones climáticas recientes y disponibilidad hídrica en los Andes Centrales Argentino–Chilenos (1885–1996). El uso de datos periodísticos para la reconstitución del clima. Meteorológica 25:27–43

Prieto MR, Herrera R, Dussel P, Gimeno L, Ribera P, Garcia R, Hernandez E (2001b) Interannual oscillations and trend of snow occurrence in the Andes region since 1885. Aust Meteorol Mag 50:164–168

Quinn WH, Neal VT (1992) The historical record of El Niño events. In: Bradley R, Jones PD (eds) Climate since A.D. 1500. Routledge, London, pp 623–648

Rabatel A, Francou B, Jomelli V, Naveau P, Grancher D (2008) A chronology of the Little Ice Age in the tropical Andes of Bolivia (16 degrees S) and its implications for climate reconstruction. Quat Res 70:198–212

Riedwyl N, Luterbacher J, Wanner H (2008) An ensemble of European summer, winter temperature reconstructions back to 1500. Geophys Res Lett 35:L20707

Riedwyl N, Küttel M, Luterbacher J, Wanner H (2009) Comparison of climate field reconstruction techniques: application to Europe. Clim Dyn 32:381–395

Röthlisberger F (1986) 10000 Jahre Gletschergeschichte der Erde, Verlag Sauerländer, Aarau

Rutherford S, Mann ME, Osborn TJ, Bradley RS, Briffa KR, Hughes MK, Jones PD (2005) Proxy-based Northern Hemisphere surface temperature reconstructions: sensitivity to method, predictor network, target season, and target domain. J Clim 18:2308–2329

Schaefer JM et al (2009) High-frequency holocene glacier fluctuations in New Zealand differ from the northern signature. Science 324:622–625

Scherrer SC, Appenzeller C (2006) Swiss Alpine snow pack variability: major patterns and links to local climate and large-scale flow. Clim Res 32:187–199

Schmelter A (2000) Climatic response and growth-trends of Nothofagus pumilio along altitudinal gradients from arid to humid sites in northern Patagonia—a progress report. In: Roig F (ed) Dendrochronología en América Latina. Editorial Nacional de Cuyo, Mendoza, pp 193–215

Schneider T (2001) Analysis of incomplete climate data: Estimation of mean values and covariance matrices and imputation of missing values. J Clim 14:853–871

Solíz C, Villalba R, Argollo J, Morales MS, Christie DA, Moya J, Pacajes J (2009) Spatio-temporal variations in Polylepis tarapacana radial growth across the Bolivian Altiplano during the 20th century. Palaeogeogr Palaeoclimatol Palaeoecol 281:296–308

Srur AM, Villalba R, Villagra PE, Hertel D (2008) Influences of climatic and CO_2 concentration changes on radial growth of Nothofagus pumilio in Patagonia. Revista Chilena De Historia Natural 81:239–256

Stahle DW et al (1998) Experimental dendroclimatic reconstruction of the Southern Oscillation. Bull Am Meteorol Soc 79:2137–2152

Stenni B, Proposito M, Gragnani R, Flora O, Jouzel J, Falourd S, Frezzotti M (2002) Eight centuries of volcanic signal and climate change at Talos Dome (East Antarctica). J Geophys Res 107:4076

Stine S (1994) Extreme and persistent drought in California and Patagonia during medieval time. Nature 369:546–549

Szeicz JM, Lara A, Díaz S, Aravena JC (2000) Dendrochronological studies of Pilgerodendron uviferum in southern South America. In: Roig F (ed) Dendrochronología en América Latina. Editorial Nacional de Cuyo, Mendoza, pp 245–270

Taulis E (1934) De la distribution des pluies au Chili. Materiaux pour l'étude des calamités 33:3–20

Thompson LG, Mosley-Thompson E, Henderson KA (2000) Ice-core palaeoclimate records in tropical South America since the Last Glacial Maximum. J Quat Sci 15:377–394
Thompson LG et al (2006) Abrupt tropical climate change: Past and present. Proc Natl Acad Sci USA 103:10536–10543
Van Ommen T. D., Morgan V., Curran M. A. J. (2004), Deglacial and Holocene changes in accumulation at Law Dome, East Antarctica, in Annals of Glaciology, vol 39, 2005, edited, Int Glaciological Soc, Cambridge, pp 359–365
Vargas WM, Naumann G (2008) Impacts of climatic change and low frequency variability in reference series on daily maximum and minimum temperature in southern South America. Reg Environ Chang 8:45–57
Villalba R (1990) Climatic fluctuations in Northern Patagonia during the last 1000 years as inferred from tree-ring records. Quat Res 34:346–360
Villalba R (1994) Tree-ring and glacial evidence for the medieval warm epoch and the little ice-age in southern South-America. Clim Change 26:183–197
Villalba R, Leiva JC, Rubulls S, Suarez J, Lenzano L (1990) Climate, tree-ring, and glacial fluctuations in the Rio Frias Valley, Rio-Negro, Argentina. Arct Alp Res 22:215–232
Villalba R, Holmes RL, Boninsegna JA (1992) Spatial patterns of climate and tree growth variations in subtropical Northwestern Argentina. J Biogeogr 19:631–649
Villalba R, Boninsegna JA, Veblen TT, Schmelter A, Rubulis S (1997a) Recent trends in tree-ring records from high elevation sites in the Andes of northern Patagonia. Clim Change 36:425–454
Villalba R, Cook ER, Darrigo RD, Jacoby GC, Jones PD, Salinger MJ, Palmer J (1997b) Sea-level pressure variability around Antarctica since AD 1750 inferred from subantarctic tree-ring records. Clim Dyn 13:375–390
Villalba R et al (2003) Large-scale temperature changes across the southern Andes: 20th-century variations in the context of the past 400 years. Clim Change 59:177–232
Villalba R, Grosjean M, Kiefer T (2009) Long-term multi-proxy climate reconstructions and dynamics in South America (LOTRED-SA): state of the art and perspectives. Palaeogeogr Palaeoclimatol Palaeoecol 281:175–179
Vimeux F, Ginot P, Schwikowski M, Vuille M, Hoffmann G, Thompson LG, Schotterer U (2009) Climate variability during the last 1000 years inferred from Andean ice cores: a review of methodology and recent results. Palaeogeogr Palaeoclimatol Palaeoecol 281:229–241
von Gunten L, Grosjean M, Rein B, Urrutia R, Appleby P (2009) A quantitative high-resolution summer temperature reconstruction based on sedimentary pigments from Laguna Aculeo, Central Chile, back to AD 850. Holocene 19:873–881
von Storch H, Zorita E, Jones JM, Dimitriev Y, Gonzalez-Rouco F, Tett SFB (2004) Reconstructing past climate from noisy data. Science 306:679–682
von Storch H, Zorita E, Gonzalez-Rouco F (2009) Assessment of three temperature reconstruction methods in the virtual reality of a climate simulation. Int J Earth Sci 98:67–82
Wanner H et al (2008) Mid- to Late Holocene climate change: an overview. Quat Sci Rev 27:1791–1828
Xoplaki E, Luterbacher J, Paeth H, Dietrich D, Steiner N, Grosjean M, Wanner H (2005) European spring and autumn temperature variability and change of extremes over the last half millennium. Geophys Res Lett 32:L15713

Supplementary Material

Article: Multiproxy multi-centennial summer and winter surface temperature field reconstructions for southern South America

Journal: Climate Dynamics

Authors: R. Neukom (corresponding author), J. Luterbacher, R. Villalba, M. Küttel, D. Frank, P. D. Jones, M. Grosjean, H. Wanner, J. C. Aravena, D. E. Black, D. A. Christie, R. D'Arrigo, A. Lara, M. Morales, C. Soliz-Gamboa, A. Srur, R. Urrutia, L. von Gunten

Affiliations of the corresponding author: Oeschger Centre for Climate Change Research (OCCR), University of Bern, Switzerland and Institute of Geography, Climatology and Meteorology, University of Bern, Switzerland

E-mail address of the corresponding author: neukom@giub.unibe.ch

This Supplementary file is structured as follows:

1. Processing of the predictor data (supplementary text)
2. Selection of the predictor sets used for the reconstructions (supplementary text)
3. Calculation of predictor weights (supplementary text)
4. Early part of the summer reconstruction (900-1492)
5. References
6. Supplementary Figures (Fig S1-S18)
7. Supplementary Tables (Tab S1-S4)

1. Processing of the predictor data

Some of the available predictor data (Tables S1-S3) were processed in order to be optimized for the purpose of seasonal climate reconstructions.

Instrumental data

Daily means of the instrumental data (Vargas and Naumann 2008) were obtained by averaging the daily maximum and minimum values. Seasonal values were obtained by first calculating monthly means and then averaging the monthly values of the corresponding seasons.

Corals

From the coral records (Table S3) that have a higher than annual resolution, we used bimonthly (Abrolhos, Ifaty) and seasonal (Great Barrier Reef, Secas, New Caledonia, Rarotonga) means.

Ship log data

We analyzed ship log data that were obtained from the CLIWOC (García-Herrera et al. 2005) and ICOADS (Worley et al. 2005) databases for their suitability as predictors for SSA climate. We used the pre-processed and gridded dataset from Küttel et al. (2009) covering 1750-2002. This dataset consists of individual point measurements of u and v wind vector components that were seasonally aggregated into grid boxes of 8° x 8° resolution over the world's oceans (Küttel et al. 2009). Based on the criteria defined by Küttel et al. (2009) we identified grid cells with sufficient data coverage (i.e. three available values per season).

Tree rings

The tree ring chronologies from South America (Tables S1 and S2) had been developed with different methods over the last ca. 30 years (Boninsegna et al. 2009). In order to make these data comparable and in attempt to preserve low frequency climate related variability, we reprocessed all datasets. As a basis for the establishment of the tree ring network we used the raw ring width measurements of 196 published and unpublished records (Tables S1 and S2). Only records going back further than 1901 were considered. First, for all sites a conservative detrending (using 300 year cubic spline filters) was applied to establish the chronologies for site comparisons and subsequent correlation and clustering analyses. Then, the set was divided into four sub-groups roughly representing the main climatic characters of the SSA Andes from North to South: The Altiplano (thereafter referred to as ALT), subtropical north western Argentina (NWA), the central part of SSA Andes (CAN; 30°S-45°S) and the southernmost (south of 45°S) part of the continent (SAN). In the ALT region all sites are *Polylepis tarapacana* (POTA). The NWA region is represented by *Alnus acuminata* (ALAC), *Juglans australis* (JGAU), *Cedrela angustifolia* (CEAN), *Cedrela lilloi* (CELI) and *Prosopis ferox* (PRFE). Records from the species *Adesmia horrida* (ADHO), *Adesmia uspallatensis* (ADUS), *Araucaria araucana* (ARAR), *Austrocedrus chilensis* (AUCH), *Fitzroya cupressoides* (FICU), *Nothofagus pumilio* (NOPU), and *Pilgerodendron uviferum* (PLUV) are available from the CAN region. The SAN data consist of *Nothofagus betuloides* (NOBE) and NOPU. Apart from that, two records from the Bolivian Amazonian region of the species

Centrolobium microchaete (CEMI) and *Cedrela odorata* (CEOD) were available, as well as two records of *Myrceugenia exsucca* (MYEX) from the semiarid Chilean Coast. Within the regions, the chronologies were then grouped into clusters based on the k-means method (Hartigan and Wong 1979) using correlations computed during the 1890-1972 common period of overlap. The stability of the resulting clusters was verified by changing the number of clusters and applying other clustering methods (PAM, Kaufman and Rousseeuw 1990; SANDRA, Philipp et al. 2007). The resulting 47 clusters are listed in Table S1. Although the clusters were created based on statistical procedures only, most clusters contain records of the same genus as well as from nearby sites (Table S1) and similar altitudinal ranges (not shown). The measurement series of the sites within the clusters were merged into one file and thereafter treated as an individual dataset. Sites that could not meaningfully be allocated to a cluster (due to the unique properties of the habitat or climate zone of the corresponding location or the large distance to the next site) were used as individual records in the further analyses. These records are listed in Table S2. For all datasets, mean chronologies for our reconstructions were developed using regional curve standardization, in order to preserve the low-frequency signal (RCS, Briffa et al. 1992; Esper et al. 2003). Years with a sample depth of less than five or an expressed population signal (EPS, Wigley et al. 1984) less than 0.85 were excluded. The starting and ending years of the resulting chronologies are shown in Tables S1 and S2. Spectral analysis of the chronologies showed that some *Nothofagus* records from the southernmost portion of the continent are affected by a strong seven-year cycle probably caused by periodic insect outbreaks (Aravena et al. 2002). These records, as well as chronologies which have a sample depth of less than 15, were eliminated in a final screening and thus not considered for reconstruction purposes.

2. Selection of the predictor sets used for the reconstructions

We established the set of predictors used for our summer and winter temperature reconstructions using two steps.

2.1. Identification of potential summer and winter temperature predictors

Out of the original database of 144 proxies (Tables S1-S3) that are related to SSA climate (e.g. temperature, precipitation or atmospheric pressure), we selected the predictors with temporally consistent and significant correlations with SSA summer or winter temperatures (potential predictor matrices). To evaluate the temporal stability, the 30-year running Spearman correlation coefficients of each proxy series with the 20th century instrumental CRU TS3 grid at the “best location” were calculated. As “best location” we defined the grid cell with the highest absolute correlation with the proxy over the overlapping period (between 70 and 106 years within 1901-2006). If the running correlation curve showed instabilities (i.e. changes in sign, or fluctuations in the coefficient that exceed ±0.2/decade) the relation between the proxy and the predictand was considered not stable and the proxy series was not included into the potential predictor matrix. In total, 44 (27) series were included into the potential predictor matrix for the summer (winter) temperature reconstructions. They are specified in the last two columns of Table S1 (tree ring clusters), Table S2 (individual tree ring records) and Table S3 (other records).

2.2. Selection of the final proxy sets

In a next step, we optimized the potential predictor matrices by identifying the optimal subset in terms of pre-defined reconstruction skill measures for each season. Due to computation limitations it was not possible to test all possible combinations of the available 44 (summer) and 27 (winter) temperature predictors. We therefore combined the proxies into meaningful sub-groups of maximum eight records based on their starting years. We then performed the PCR reconstructions and verifications for all possible combination of proxies within the oldest group and selected the combination with the highest skill scores. This set was then combined with all possible combinations of the next younger group and again, the set with the highest skill was evaluated. This procedure was repeated for all sub-groups. Finally, we used the leave-one-out (“add-one-more”) method to test, whether the quality could be further improved by removing (adding) some of the selected (excluded) predictors. For the SSA mean reconstructions (see Table 3 in the main text) we used the average of the RE and r^2 scores as measure for the quality. The spatial reconstructions were assessed based on the average number of grid cells with positive REs. We performed the evaluation by computing an SSA mean and a spatial reconstruction with each set and equally weighting both criteria. Independent use of the two criteria lead to two very similar predictor sets for the SSA mean and spatial reconstructions (not shown). Verification of the results by comparing the skill scores of selected subsets with the corresponding results of CPS and RegEM showed that the rankings of the subsets are relatively robust and similar for the three methods (not shown). The final set of 22 (20) summer (winter) temperature proxies and the temporal evolution of the number of predictors are presented in Table 1 (Table 2) and Figure 1 in the main text.

3. Calculation of predictor weights

For our PCR reconstructions, we calculated the weight that each predictor has at each time step and location in our regression models as described by (Briffa et al. 1986). In order to deal with the changing number of predictors over time, the sum of the weights was normalized to a value of one at each year and all weights were then multiplied with the number of predictors available in the respective year. The average weight of each predictor in four selected years for summer (winter) is shown in Figure S15 (S17) and the predictor with the largest weight at each location in the same years are displayed in Figure S16 (S18).

4. Early part of the summer reconstruction (900-1492)

In the period before 1493 only one proxy in the summer temperature reconstructions stems from inside the reconstruction area: the Laguna Aculeo lake sediment record (von Gunten et al. 2009). The other four proxies used in this timeframe stem from outside SSA and are only connected to its climate through teleconnections which are assumed to remain stable over time. Figure S8 shows, however, that the reconstruction is robust to changes in the predictor subset, also in this period. Figure S8a shows our PCR summer reconstruction along with the same reconstruction when each of the five predictors available is omitted from the proxy set. These curves mostly stay within the 2SE uncertainty bands of the original reconstruction, except for the case, when the Laguna Aculeo record is omitted. This indicates that the record from within SSA (Laguna Aculeo) is the most important proxy for the SSA mean temperature reconstruction in this time period. Figure S8b displays the PCR reconstruction together with a reconstruction using only the Laguna Aculeo record and two additional tree ring cluster chronologies (CAN 1 and CAN 6, see Table S1) from within SSA that go back beyond 1493 as predictors. These two tree ring records are part of the summer temperature predictors that were excluded from the “optimal set” and retained for validation (Figure 9a). This reconstruction, which is based on SSA predictors only, shows very similar decadal-scale fluctuations as the original reconstruction, albeit with larger amplitudes and lower skill (not shown). Over all, Figure S8 indicates that the reconstructed temperatures are very probably reflecting realistic SSA climate variations also in the early part of the reconstruction, where few predictors are available.

5. References

Aravena J. C., Lara A., Wolodarsky-Franke A., Villalba R., Cuq E. (2002) Tree-ring growth patterns and temperature reconstruction from Nothofagus pumilio (Fagaceae) forests at the upper tree line of southern Chilean Patagonia. Revista Chilena De Historia Natural 75: 361-376

Argollo J., Solìz C., Villalba R. (2004) Potencialidad dendrocronológica de Polylepis tarapacana en los Andes Centrales de Bolivia. Ecol. Boliv. 39: 5-24

Aristarain A. J., Delmas R. J., Stievenard M. (2004) Ice-core study of the link between sea-salt aerosol, sea-ice cover and climate in the Antarctic Peninsula area. Clim. Change 67: 63-86

Black D. E., Abahazi M. A., Thunell R. C., Kaplan A., Tappa E. J., Peterson L. C. (2007) An 8-century tropical Atlantic SST record from the Cariaco Basin: Baseline variability, twentieth-century warming, and Atlantic hurricane frequency. Paleoceanography 22: PA4204

Boninsegna J. A. (1988) Santiago de Chile winter rainfall since 1220 as being reconstructed by tree rings. Quaternary South Am. 6: 67-87

Boninsegna J. A., Keegan J., Jacoby G. C., D'Arrigo R., Holmes R. L. (1989) Dendrochronological studies in Tierra del Fuego, Argentina. Quaternary South Am. 7: 315-326

Boninsegna J. A., et al. (2009) Dendroclimatological reconstructions in South America: A review. Palaeogeogr. Palaeoclimatol. 281: 210-228

Brienen R. J. W., Zuidema P. A. (2005) Relating tree growth to rainfall in Bolivian rain forests: a test for six species using tree ring analysis. Oecologia 146: 1-12

Briffa K. R., Jones P. D., Wigley T. M., Pilcher J. R., Baillie M. (1986) Climate Reconstruction from Tree Rings: Part 2, spatial Reconstruction of Summer Mean Sea-Level Pressure Patterns over Great Britain. J. Climatol. 6: 1-15

Briffa K. R., et al. (1992) Fennoscandian Summers from Ad-500 - Temperature-Changes on Short and Long Timescales. Clim. Dynam. 7: 111-119

Christie D. A., Lara A., Barichivich J., Villalba R., Morales M. S., Cuq E. (2009) El Niño-Southern Oscillation signal in the world's highest-elevation tree-ring chronologies from the Altiplano, Central Andes. Palaeogeogr. Palaeoclimatol. 281: 309-319

Cook E. R., Palmer J. G., D'Arrigo R. D. (2002) Evidence for a 'Medieval Warm Period' in a 1,100 year tree-ring reconstruction of past austral summer temperatures in New Zealand. Geophys. Res. Lett. 29: 1667

D'Arrigo R., et al. (2006) Monsoon drought over Java, Indonesia, during the past two centuries. Geophys. Res. Lett. 33: L04709

Dunbar R. B., Wellington G. M., Colgan M. W., Glynn P. W. (1994) Eastern Pacific Sea-Surface Temperature since 1600-AD - the Delta-O-18 Record of Climate Variability in Galapagos Corals. Paleoceanography 9: 291-315

Esper J., Cook E. R., Krusic P. J., Peters K., Schweingruber F. H. (2003) Tests of the RCS method for preserving low-frequency variability in long tree-ring chronologies. Tree-Ring Research 59: 81-98

García-Herrera R., Konnen G. P., Wheeler D. A., Prieto M. R., Jones P. D., Koek F. B. (2005) CLIWOC: A climatological database for the world's oceans 1750-1854. Clim. Change 73: 1-12

García-Herrera R., et al. (2008) A Chronology of El Niño Events from Primary Documentary Sources in Northern Peru. J. Clim. 21: 1948-1962

Gioda A., Prieto M. R. (1999a) Para una historia climática de La Paz en los últimos cinco siglos. Historias de la ciudad de La Paz, Bolivia. Revista de la coordinadora de Historia 3: 13-33
Gioda A., Prieto M. R. (1999b) Histoire des sécheresses andines. Potosí, El Niño et le Petit Age Glaciaire. Revue de la Société Météorologique de France. La Météorologie 27: 33-42
Graf W., Oerter H., Reinwarth O., Stichler W., Wilhelms F., Miller H., Mulvaney R. (2002) Stable-isotope records from Dronning Maud Land, Antarctica. Ann. Glaciol. 35: 195-201
Hartigan J. A., Wong M. A. (1979) Algorithm AS 136: A K-Means Clustering Algorithm. Journal of the Royal Statistical Society. Series C (Applied Statistics) 28: 100-108
Herrera R., Prieto M. R., García-Herrera R. (2003), Floods in the semiarid Argentinean Chaco during the 17th to 19th centuries, in *Proceedings of Palaeofloods, Historical Data & Climatic Variability: Applications in Flood Risk Assessment*, edited by V. R. Thorndycraft, et al., pp. 107-112, CSIC-Centro de Ciencias Medioambientales, Madrid.
Kaufman L., Rousseeuw P. J. (1990), *Finding Groups in Data: An Introduction to Cluster Analysis*, John Wiley & Sons, Inc., New York.
Kellerhals T. (2008), Holocene climate fluctuations in tropical South America deduced from an Illimani ice core, Dissertation, University of Bern, Switzerland.
Kuhnert H., et al. (1999) A 200-year coral stable oxygen isotope record from a high-latitude reef off western Australia. Coral Reefs 18: 1-12
Küttel M., et al. (2009) The importance of ship log data: reconstructing North Atlantic, European and Mediterranean sea level pressure fields back to 1750. Clim. Dynam.: doi:10.1007/s00382-00009-00577-00389
Lamarche V. C., Holmes R. L., Dunwiddie P. W., Drew L. G. (1979a), *Tree-ring chronologies of the southern hemisphere: Vol. 1: Argentina. Chronology Series V*, Laboratory of Tree-Ring Research, University of Arizona, Tuczon, AZ.
Lamarche V. C., Holmes R. L., Dunwiddie P. W., Drew L. G. (1979b), *Tree-ring chronologies of the southern hemisphere: Vol. 2: Chile. Chronology Series V*, Laboratory of Tree-Ring Research, University of Arizona, Tuczon, AZ.
Lara A., Villalba R. (1993) A 3620-Year Temperature Record from Fitzroya-Cupressoides Tree Rings in Southern South-America. Science 260: 1104-1106
Lara A., Villalba R., Aravena J. C., Wolodarsky A., Neira A. (2000), Desarollo de una red de cronologías de Fitzroya Cupressoides (Alerce) para Chile y Argentina, in *Dendrochronología en América Latina*, edited by F. Roig, pp. 193-215, Editorial Nacional de Cuyo, Mendoza.
Lara A., Aravena J. C., Villalba R., Wolodarsky-Franke A., Luckman B., Wilson R. (2001) Dendroclimatology of high-elevation Nothofagus pumilio forests at their northern distribution limit in the central Andes of Chile. Can. J. Forest. Res. 31: 925-936
Lara A., Villalba R., Wolodarsky-Franke A., Aravena J. C., Luckman B. H., Cuq E. (2005) Spatial and temporal variation in Nothofagus pumilio growth at tree line along its latitudinal range (35 degrees 40 '-55 degrees S) in the Chilean Andes. J. Biogeogr. 32: 879-893
Lara A., Villalba R., Urrutia R. (2008) A 400-year tree-ring record of the Puelo River summer-fall streamflow in the Valdivian Rainforest eco-region, Chile. Clim. Change 86: 331-356
Linsley B. K., Wellington G. M., Schrag D. P. (2000) Decadal sea surface temperature variability in the subtropical South Pacific from 1726 to 1997 AD. Science 290: 1145-1148

Linsley B. K., Zhang P. P., Kaplan A., Howe S. S., Wellington G. M. (2008) Interdecadal-decadal climate variability from multicoral oxygen isotope records in the South Pacific Convergence Zone region since 1650 A.D. Paleoceanography 23: PA2219
Lough J. M. (2007) Tropical river flow and rainfall reconstructions from coral luminescence: Great Barrier Reef, Australia. Paleoceanography 22: PA2218
Masiokas M., Villalba R. (2004) Climatic significance of intra-annual bands in the wood of Nothofagus pumilio in southern Patagonia. Trees-Struct. Funct. 18: 696-704
McCulloch M., Fallon S., Wyndham T., Hendy E., Lough J., Barnes D. (2003) Coral record of increased sediment flux to the inner Great Barrier Reef since European settlement. Nature 421: 727-730
Mitchell T. D., Jones P. D. (2005) An improved method of constructing a database of monthly climate observations and associated high-resolution grids. Int. J. Climatol. 25: 693-712
Morales M. S., Villalba R., Grau H. R., Paolini L. (2004) Rainfall-controlled tree growth in high-elevation subtropical treelines. Ecology 85: 3080-3089
Mundo I. A., Barrera M. D., Roig F. A. (2007) Testing the utility of Nothofagus pumilio for dating a snow avalanche in Tierra del Fuego, Argentina. Dendrochronologia 25: 19-28
Nan S., Li J. (2003) The relationship between the summer precipitation in the Yangtze River valley and the boreal spring Southern Hemisphere annular mode. Geophys. Res. Lett. 30
Neukom R., et al. (2009) An extended network of documentary data from South America and its potential for quantitative precipitation reconstructions back to the 16th century. Geophys. Res. Lett. 36: L12703
Philipp A., Della-Marta P. M., Jacobeit J., Fereday D. R., Jones P. D., Moberg A., Wanner H. (2007) Long-term variability of daily North Atlantic-European pressure patterns since 1850 classified by simulated annealing clustering. J. Clim. 20: 4065-4095
Prieto M. R., Herrera R., Dussel P. (1999a) Snowfall and floods in the oriental slope of Argentinean–Chilean Andes from the Middle of the 18th century to the End the 19th century. Its relationship with ENSO. Extended Abstract. Conference on Reconstructing Climatic variability from Historical Sources and Other Proxy Records. Earth System History Program of the U. S NSF and the Office of Global Programs of the U.S NOAA, Manzanillo , México.
Prieto M. R., Herrera R., Dussel P. (1999b) Historical evidences of streamflow fluctuations in the Mendoza River, Argentina, and their relationship with ENSO. Holocene 9: 473-481
Prieto M. R., Herrera R., Dussel P. (2000), Archival evidence for some aspects of historical climate variability in Argentina and Bolivia during the 17th and 18th centuries., in *Southern Hemisphere Paleo and Neo-Climates: Methods and Concepts*, edited by P. P. Smolka and W. Volkheimer, pp. 127-142, Springer, Berlin.
Prieto M. R., Herrera R., Castrillejo T., Dussel P. (2001a) Variaciones climáticas recientes y disponibilidad hídrica en los Andes Centrales Argentino–Chilenos (1885-1996). El uso de datos periodísticos para la reconstitución del clima. Meteorológica 25: 27-43
Prieto M. R., Herrera R., Dussel P., Gimeno L., Ribera P., Garcia R., Hernandez E. (2001b) Interannual oscillations and trend of snow occurrence in the Andes region since 1885. Aust. Meteorol. Mag. 50: 164-168
Prieto M. R. (2007) ENSO signals in South America: rains and floods in the Parana River region during colonial times. Clim. Change 83: 39-54
Quinn T. M., Crowley T. J., Taylor F. W., Henin C., Joannot P., Join Y. (1998) A multicentury stable isotope record from a New Caledonia coral: Interannual and decadal sea surface temperature variability in the southwest Pacific since 1657 AD. Paleoceanography 13: 412-426

Quinn W. H., Neal V. T. (1992), The historical record of El Niño events, in *Climate since A.D. 1500*, edited by R. Bradley and P. D. Jones, pp. 623-648, Routledge, London.
Ramirez E., et al. (2003) A new Andean deep ice core from Nevado Illimani (6350 m), Bolivia. Earth and Planetary Science Letters 212: 337-350
Rasbury M., Aharon P. (2006) ENSO-controlled rainfall variability records archived in tropical stalagmites from the mid-ocean island of Niue, South Pacific. Geochem. Geophys. Geosyst. 7: Q07010
Rein B., Luckge A., Sirocko F. (2004) A major Holocene ENSO anomaly during the Medieval period. Geophys. Res. Lett. 31: L17211
Roig F., Boninsegna J. (1990) Environmental factors affecting growth of Adesmia communities as determined from tree rings. Dendrochronologia 8: 39-65
Roig F. A., Boninsegna J. A. (1991) Studies on Radial, Basal and Height Growth, and Climate-Growth Relationships in Pilgerodendron-Uviferum. Revista Chilena De Historia Natural 64: 53-63
Schmelter A. (2000), Climatic response and growth-trends of Nothofagus pumilio along altitudinal gradients from arid to humid sites in northern Patagonia - A progress report, in *Dendrochronología en América Latina*, edited by F. Roig, pp. 193-215, Editorial Nacional de Cuyo, Mendoza.
Schneider D. P., Steig E. J., van Ommen T. D., Dixon D. A., Mayewski P. A., Jones J. M., Bitz C. M. (2006) Antarctic temperatures over the past two centuries from ice cores. Geophys. Res. Lett. 33: L16707
Solíz C., Villalba R., Argollo J., Morales M. S., Christie D. A., Moya J., Pacajes J. (2009) Spatio-temporal variations in Polylepis tarapacana radial growth across the Bolivian Altiplano during the 20th century. Palaeogeogr. Palaeoclimatol. 281: 296-308
Srur A. M., Villalba R., Villagra P. E., Hertel D. (2008) Influences of climatic and CO2 concentration changes on radial growth of Nothofagus pumilio in Patagonia. Revista Chilena De Historia Natural 81: 239-256
Stahle D. W., et al. (1998) Experimental dendroclimatic reconstruction of the Southern Oscillation. Bull. Amer. Meteorol. Soc. 79: 2137-2152
Stenni B., Proposito M., Gragnani R., Flora O., Jouzel J., Falourd S., Frezzotti M. (2002) Eight centuries of volcanic signal and climate change at Talos Dome (East Antarctica). J. Geophys. Res. 107: 4076
Szeicz J. M., Lara A., Díaz S., Aravena J. C. (2000), Dendrochronological studies of Pilgerodendron uviferum in southern South America, in *Dendrochronología en América Latina*, edited by F. Roig, pp. 245-270, Editorial Nacional de Cuyo, Mendoza.
Taulis E. (1934) De la distribution des pluies au Chili. Materiaux pour l'étude des calamités 33: 3-20
Thomas E. R., Marshall G. J., McConnell J. R. (2008) A doubling in snow accumulation in the western Antarctic Peninsula since 1850. Geophys. Res. Lett. 35: L01706
Thompson L. G., Mosley-Thompson E., Henderson K. A. (2000) Ice-core palaeoclimate records in tropical South America since the Last Glacial Maximum. J. Quat. Sci. 15: 377-394
Thompson L. G., et al. (2006) Abrupt tropical climate change: Past and present. Proc. Natl. Acad. Sci. U. S. A. 103: 10536-10543
Van Ommen T. D., Morgan V., Curran M. A. J. (2004), Deglacial and Holocene changes in accumulation at Law Dome, East Antarctica, in *Annals of Glaciology, Vol 39, 2005*, edited, pp. 359-365, Int Glaciological Soc, Cambridge.
Vargas W. M., Naumann G. (2008) Impacts of climatic change and low frequency variability in reference series on daily maximum and minimum temperature in southern South America. Reg. Envir. Chang. 8: 45-57

Villalba R. (1990) Latitude of the surface high-pressure belt over western South America during the last 500 years as inferred from tree-ring analysis. Quaternary South Am. 7: 273-303

Villalba R., Leiva J. C., Rubulls S., Suarez J., Lenzano L. (1990) Climate, Tree-Ring, and Glacial Fluctuations in the Rio Frias Valley, Rio-Negro, Argentina. Arctic and Alpine Research 22: 215-232

Villalba R., Holmes R. L., Boninsegna J. A. (1992) Spatial Patterns of Climate and Tree Growth Variations in Subtropical Northwestern Argentina. J. Biogeogr. 19: 631-649

Villalba R., Boninsegna J. A., Veblen T. T., Schmelter A., Rubulis S. (1997) Recent trends in tree-ring records from high elevation sites in the Andes of northern Patagonia. Clim. Change 36: 425-454

Villalba R., Veblen T. T. (1997) Spatial and temporal variation in Austrocedrus growth along the forest-steppe ecotone in northern Patagonia. Can. J. Forest. Res. 27: 580-597

Villalba R., Cook E. R., Jacoby G. C., D'Arrigo R. D., Veblen T. T., Jones P. D. (1998) Tree-ring based reconstructions of northern Patagonia precipitation since AD 1600. Holocene 8: 659-674

Vimeux F., Ginot P., Schwikowski M., Vuille M., Hoffmann G., Thompson L. G., Schotterer U. (2009) Climate variability during the last 1000 years inferred from Andean ice cores: A review of methodology and recent results. Palaeogeography, Palaeoclimatology, Palaeoecology 281: 229-241

von Gunten L., Grosjean M., Rein B., Urrutia R., Appleby P. (2009) A quantitative high-resolution summer temperature reconstruction based on sedimentary pigments from Laguna Aculeo, Central Chile, back to AD 850. Holocene 19: 873-881

Wigley T. M. L., Briffa K. R., Jones P. D. (1984) On the Average Value of Correlated Time-Series, with Applications in Dendroclimatology and Hydrometeorology. Journal of Climate and Applied Meteorology 23: 201-213

Wolter K., Timlin M. S. (1998) Measuring the strength of ENSO events –- how does 1997/98 rank? Weather 53: 315-324

Worley S. J., Woodruff S. D., Reynolds R. W., Lubker S. J., Lott N. (2005) ICOADS release 2.1 data and products. Int. J. Climatol. 25: 823-842

Zinke J., Dullo W. C., Heiss G. A., Eisenhauer A. (2004) ENSO and Indian Ocean subtropical dipole variability is recorded in a coral record off southwest Madagascar for the period 1659 to 1995. Earth and Planetary Science Letters 228: 177-194

6. Supplementary Figures

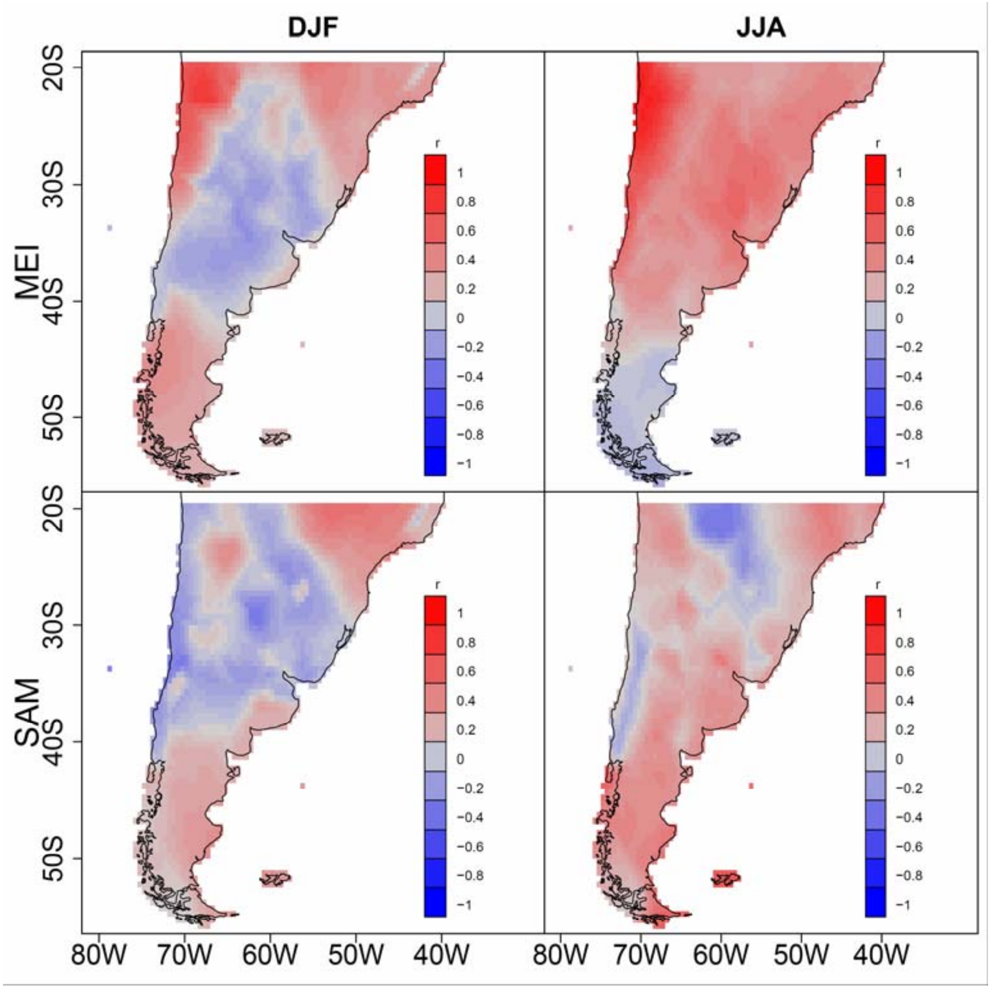

Fig. S1 Seasonal Pearson correlations of ENSO (MEI index by Wolter and Timlin 1998) and SAM (Nan and Li 2003) with SSA summer (left) and winter (right) temperature (CRU TS 3; updated from Mitchell and Jones 2005) 1950-2006.

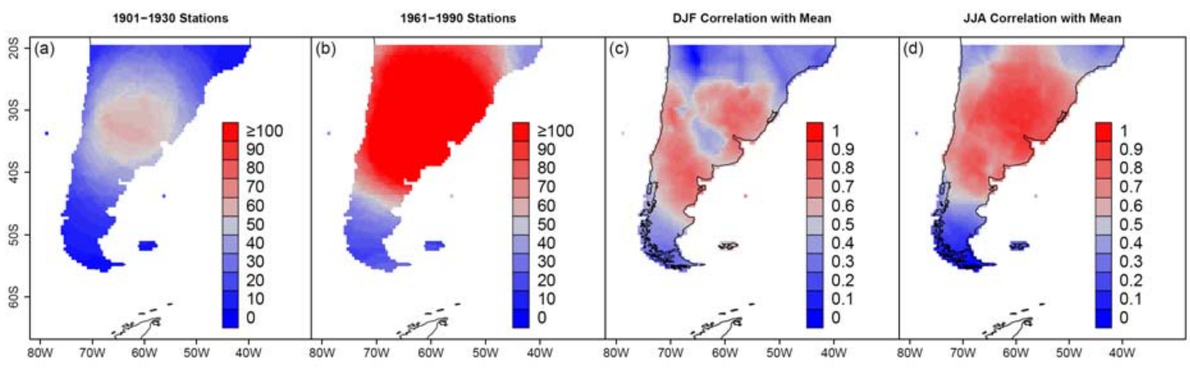

Fig. S2 Average number of instrumental stations within range of each cell of the CRU TS 2.1 temperature grid 1901-1930 (a) and 1961-1990 (b; data source: http://www.cru.uea.ac.uk/~timm/grid/CRU_TS_2_1.html).

Correlation of each grid cell of the predictand grid with the mean over all SSA 1901-1995 in summer (c) and winter (d)

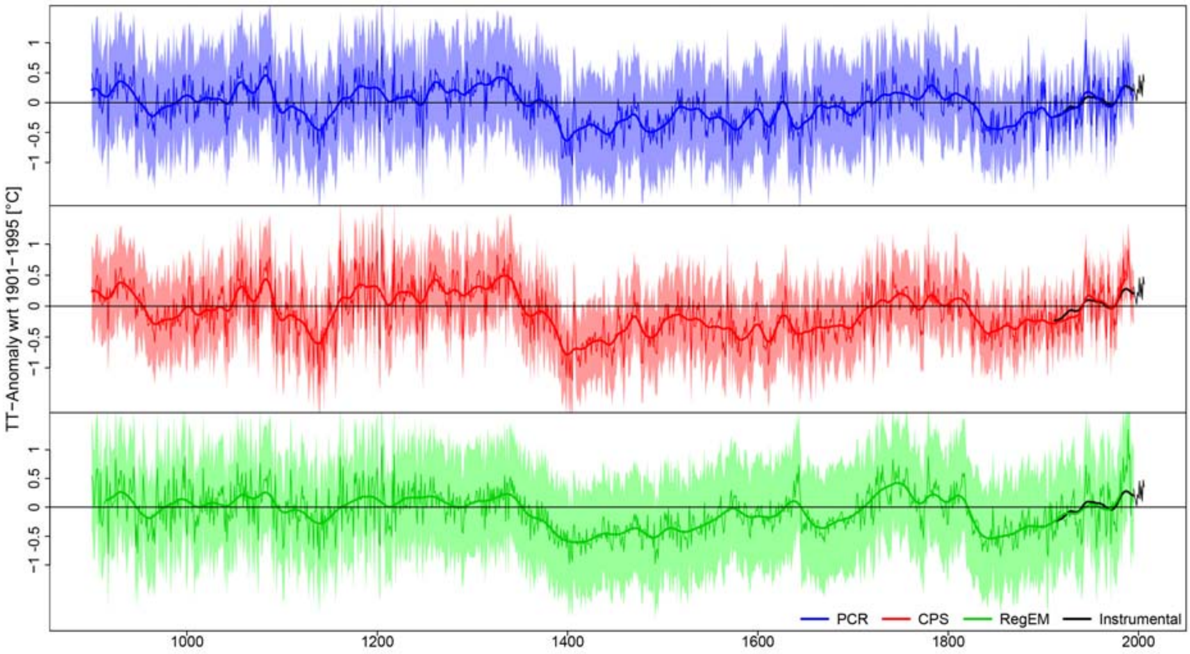

Fig. S3 Interannual variations of the PCR (top, blue), CPS (middle, red) and RegEM (bottom, green) summer temperature reconstructions 900-1995 and CRU gridded temperatures 1996-2006 (black). Thick lines are 30-year Gaussian filtered anomalies (CRU gridded data are from 1901). Shaded: interannual 2 SE bounds

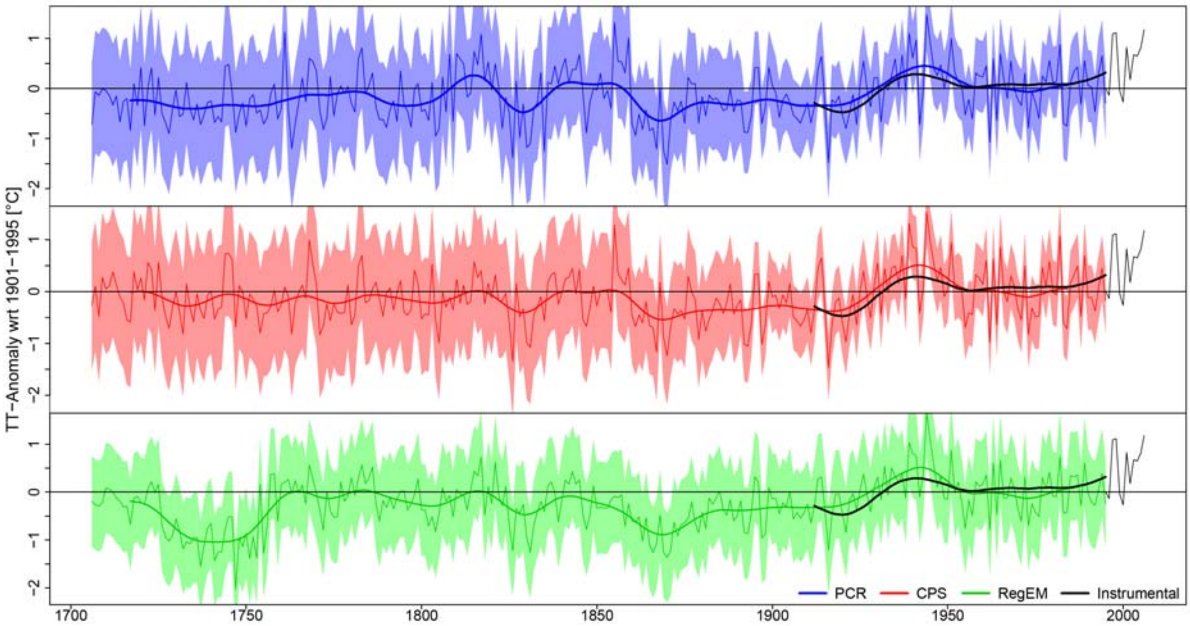

Fig. S4 Same as Fig. S3 but for winter in the period 1706-1995 and with different scale on the y axis

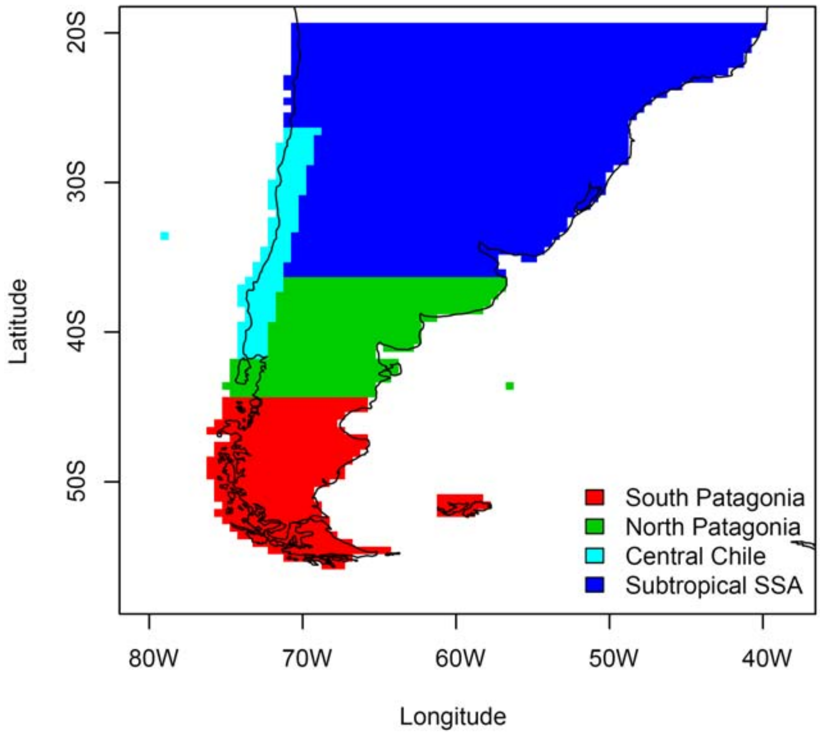

Fig. S5 The sub-regions defined for the regional analyses

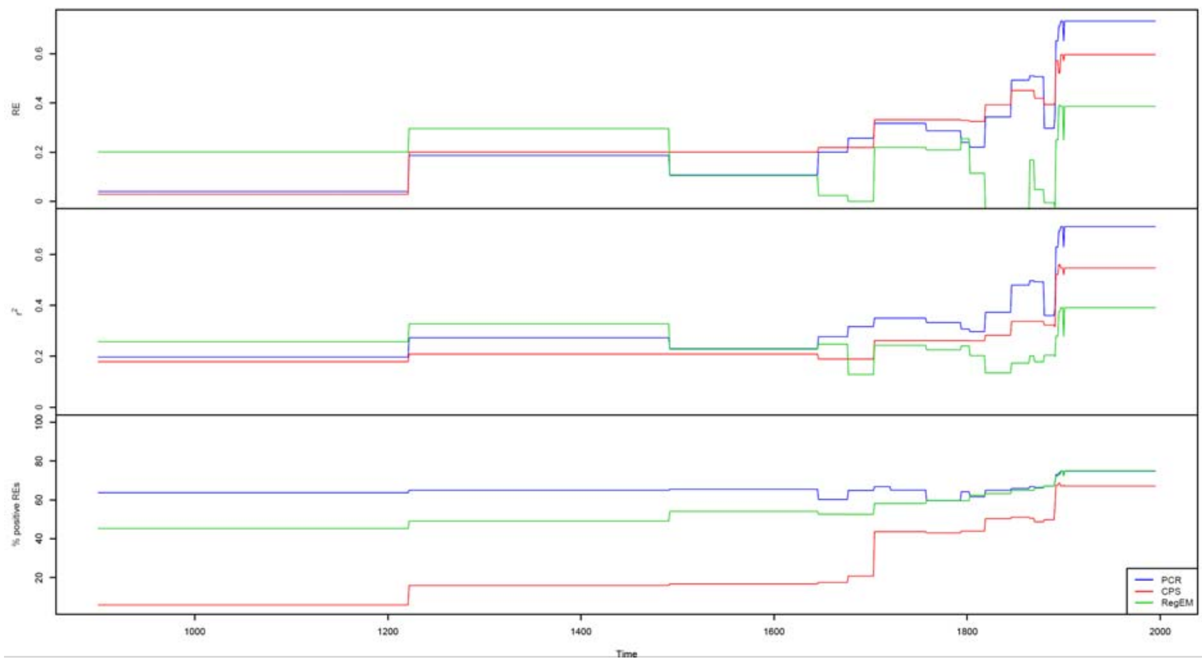

Fig. S6 Skill measures of the summer PCR (blue), CPS (red) and RegEM (green) reconstructions 900-1995. Top: REs of the SSA mean reconstructions. Middle: r^2 of the SSA mean reconstructions. Bottom: Percentage of grid cells with positive REs in the spatial reconstructions

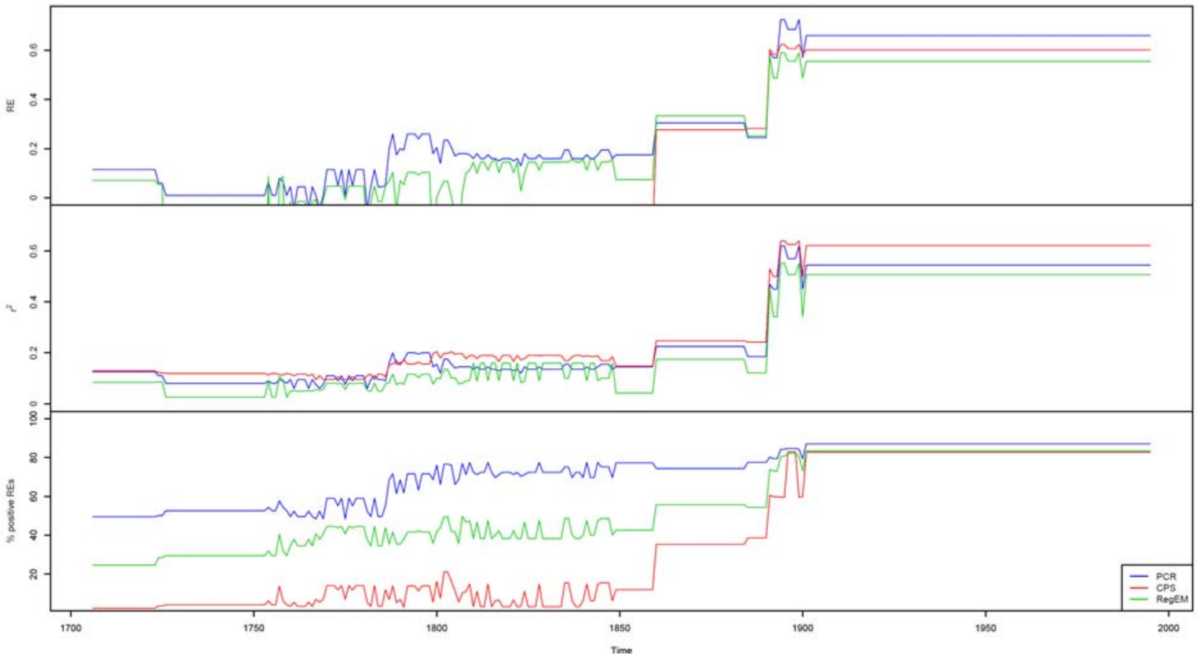

Fig. S7 Same as Fig. S6 but for winter in the period 1706-1995

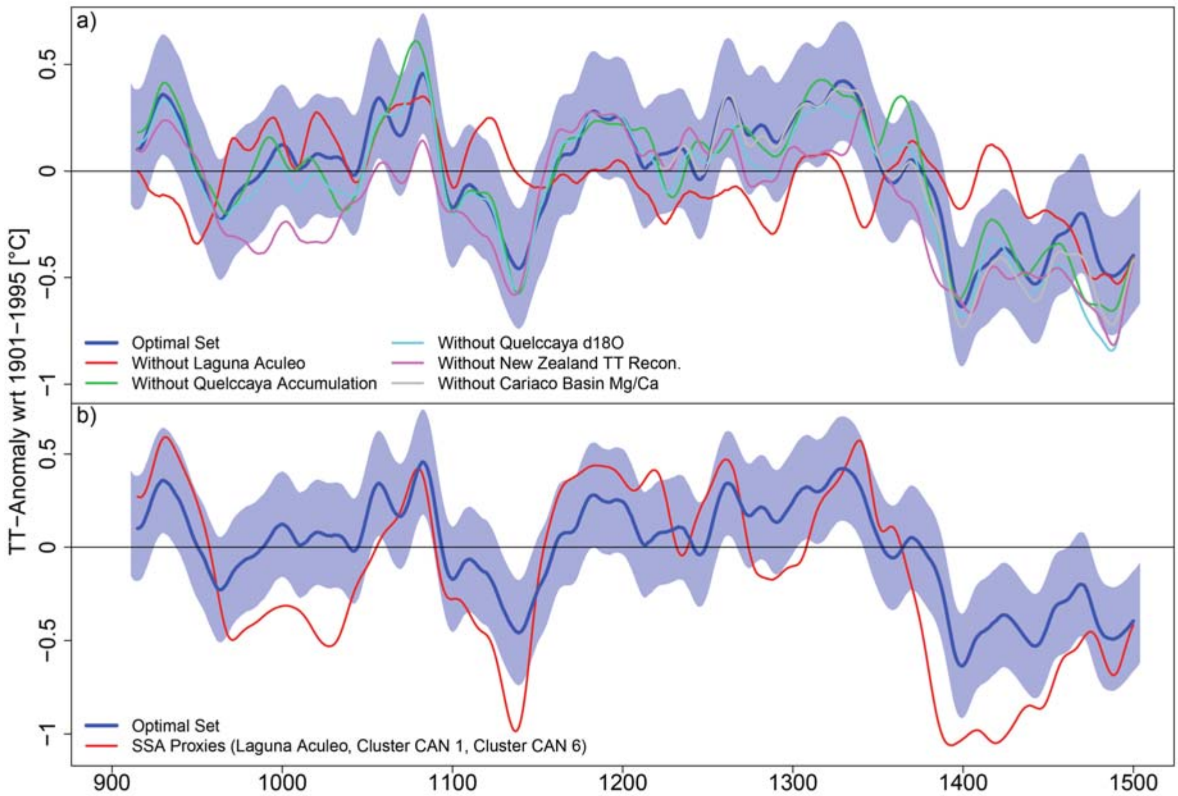

Fig. S8 30-year Gaussian filtered PCR SSA mean summer temperature reconstruction 900-1500, anomalous to the calibration period (1901-1995) mean (blue), and associated ±2SE uncertainty bands (shaded) compared to other realizations of the reconstruction based on varying predictor sets: (a) Reconstructions omitting one of the five predictors available in the pre-1493 period. (b) Reconstruction based on SSA predictors only (see text for details).

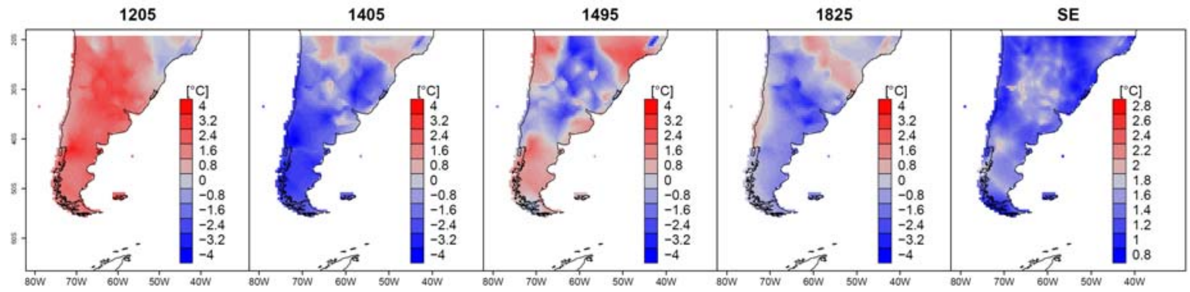

Fig. S9 First four panels: Spatial summer temperature anomalies (wrt 1901-1995), reconstructed using PCR of the years 1205 (warmest year in reconstruction period), 1405 (coldest year in reconstruction period), 1495 and 1825 (two years with pronounced regional differences). Red colors stand for positive, blue for negative anomalies. Last panel: Mean unfiltered uncertainties in the PCR reconstruction

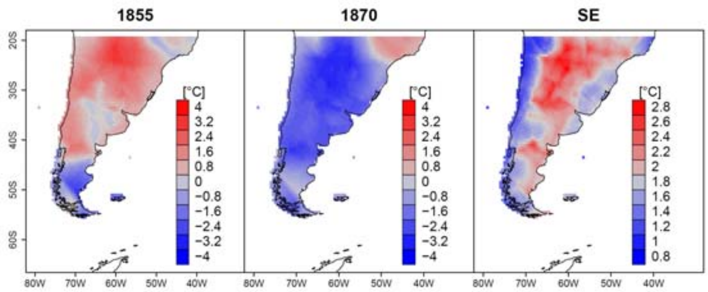

Fig. S10 Same as Fig. S9 but for the years 1855 (warmest year in reconstruction period) and 1870 (coldest year in reconstruction period) in winter

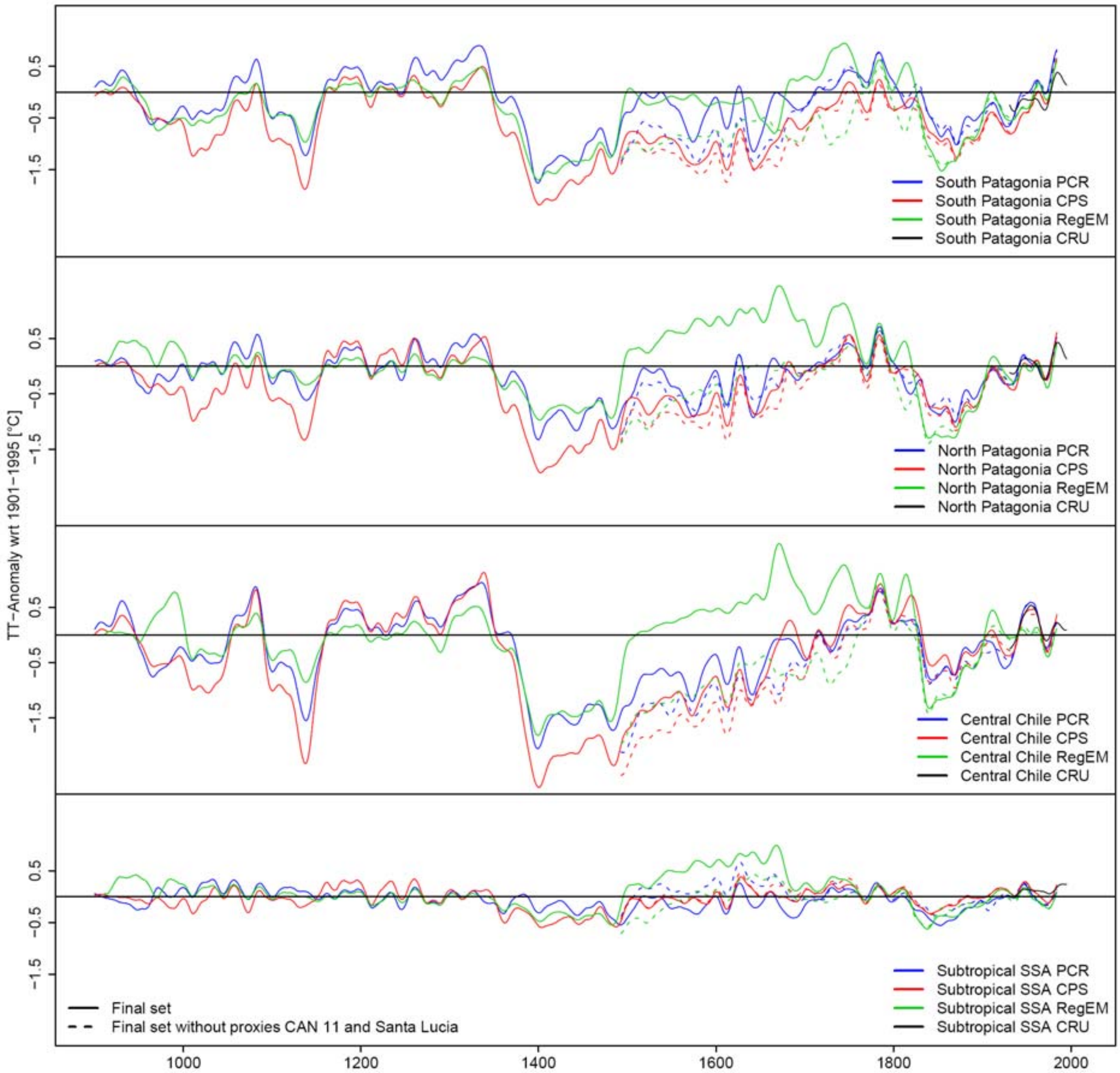

Fig. S11 Comparison of the 30-year Gaussian filtered PCR (blue), CPS (red) and RegEM (green) spatial summer reconstructions in the different sub-regions of SSA. Black: CRU gridded data. Dashed lines: Reconstructions without the tree ring proxies “CAN 11” and “Santa Lucia”

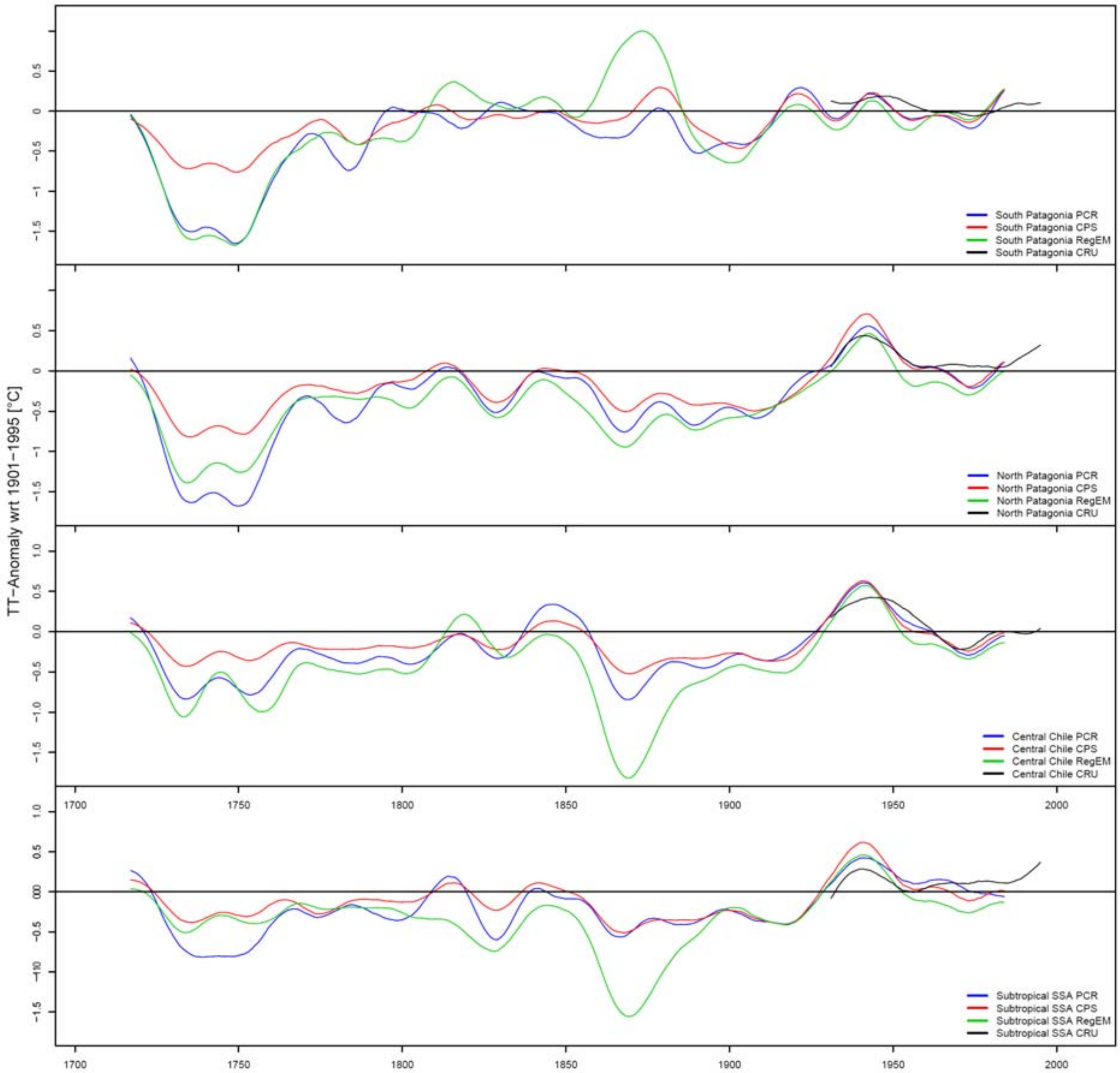

Fig. S12 Comparison of the 30-year Gaussian filtered PCR (blue), CPS (red) and RegEM (green) spatial winter reconstructions in the different sub-regions of SSA. Black: CRU gridded data

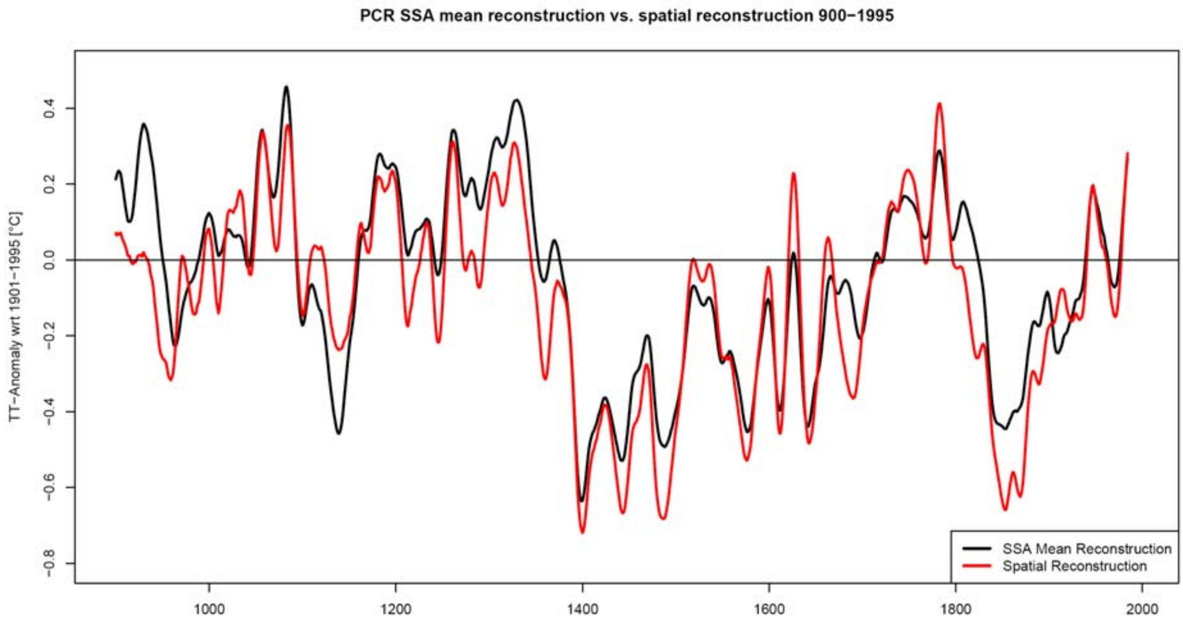

Fig. S13 Differences between the SSA mean summer reconstruction (black) and the average of the spatial summer reconstruction (red) for PCR 900-1995. The differences between the methodological setups to reconstruct these two curves are the EOF truncation parameter for the predictors (0.8 for the SSA mean and 0.85 for the spatial reconstruction, respectively) and the calibration period (1901-1995 and 1931-1995, respectively; see Table 3 in the main text)

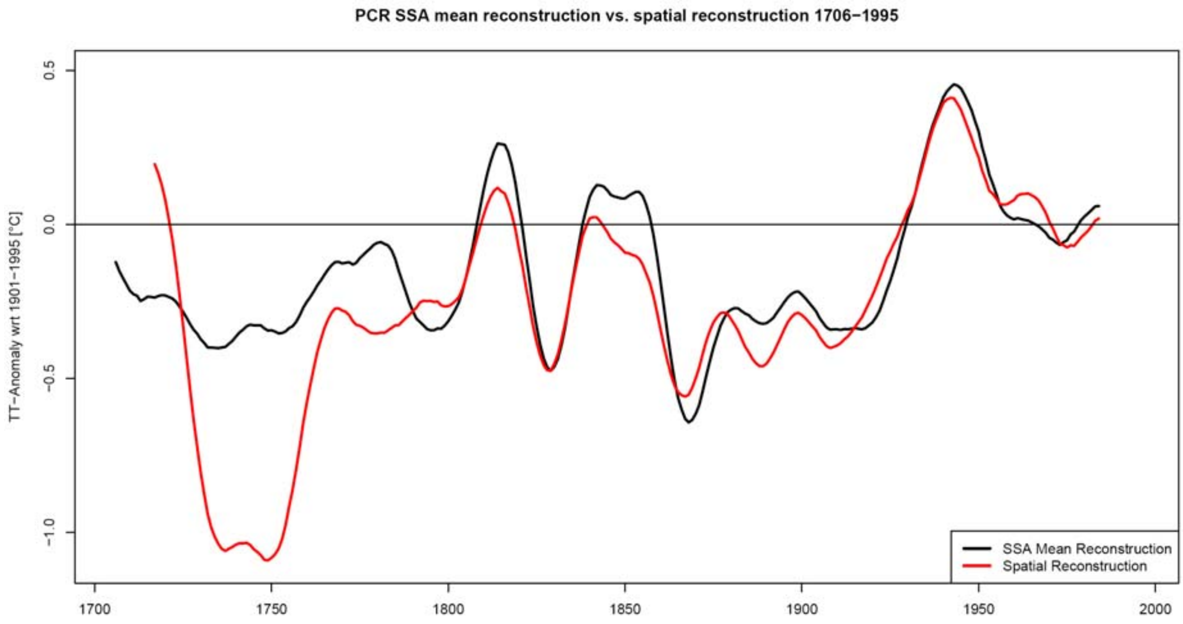

Fig. S14 Same as Fig. S13 but for winter and for the period 1706-1995.

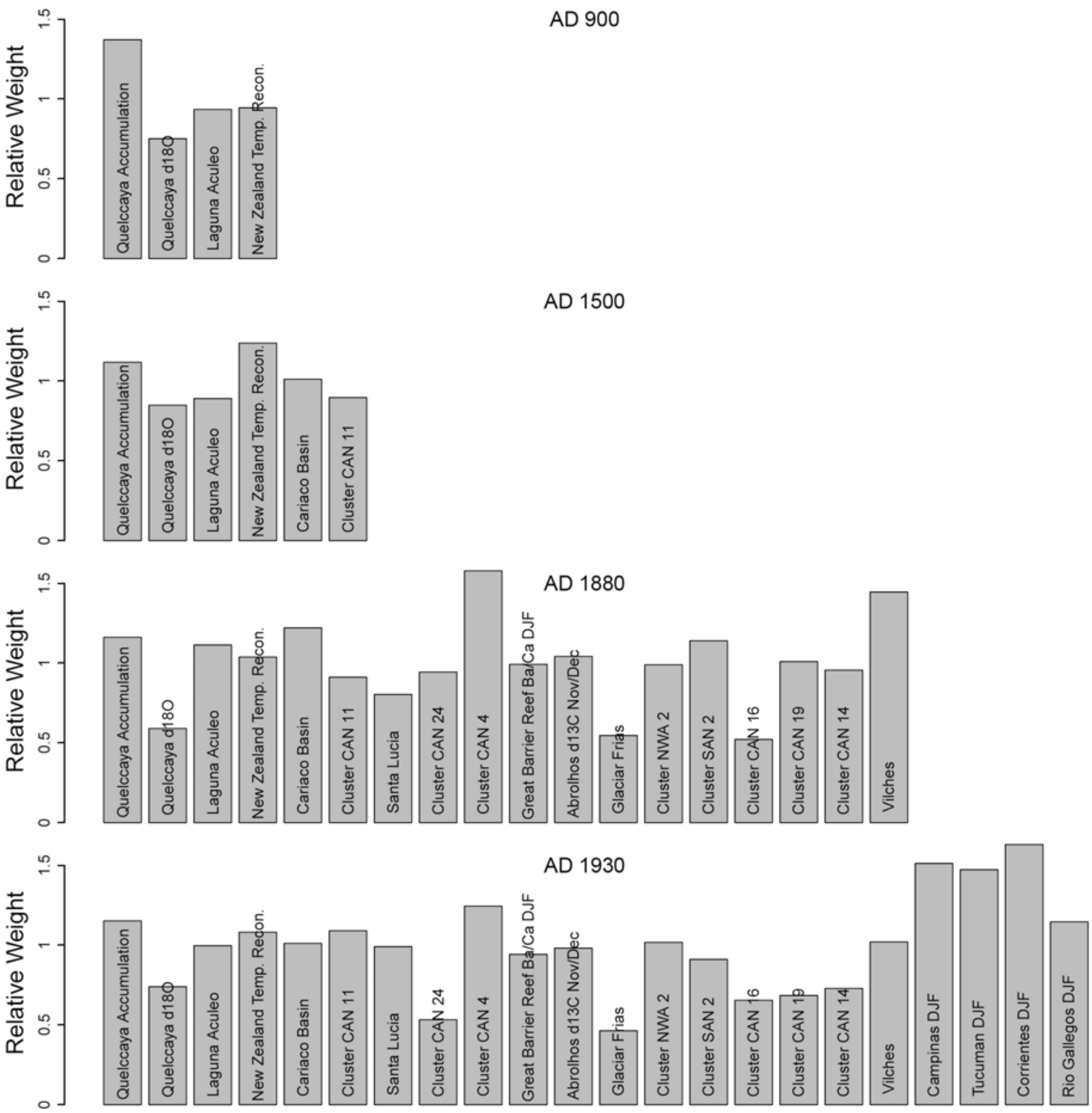

Fig. S15 Relative weight of each predictor in the PCR summer reconstruction in AD 900, AD1500, AD1880 and AD1930.

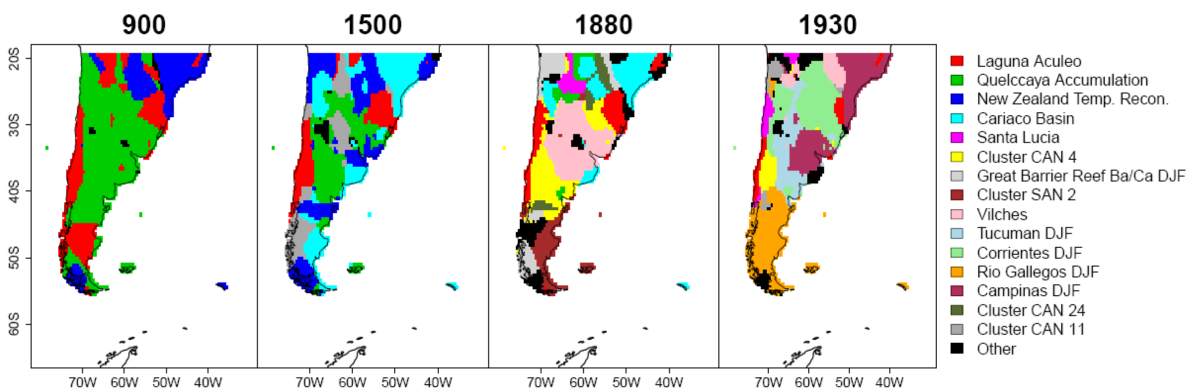

Fig. S16 Predictor with the largest regression weight at each grid cell in the PCR summer reconstruction in the years AD 900 (first panel) AD 1500 (second panel) AD 1880 (third panel) and AD 1930 (last panel)

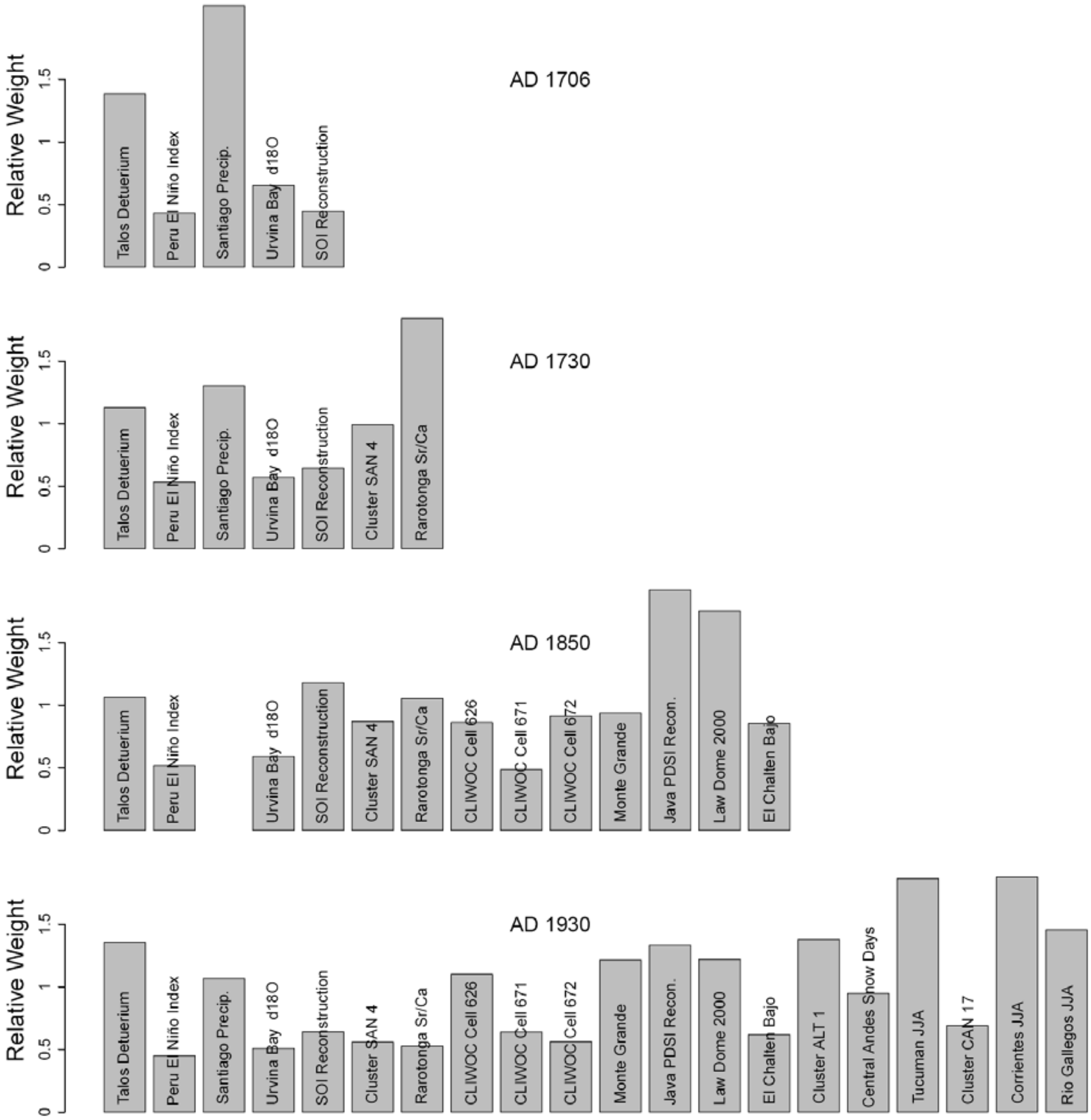

Fig. S17 Same as Fig. S15 but for winter and the years AD 1706, AD 1730, AD1850 and AD 1930

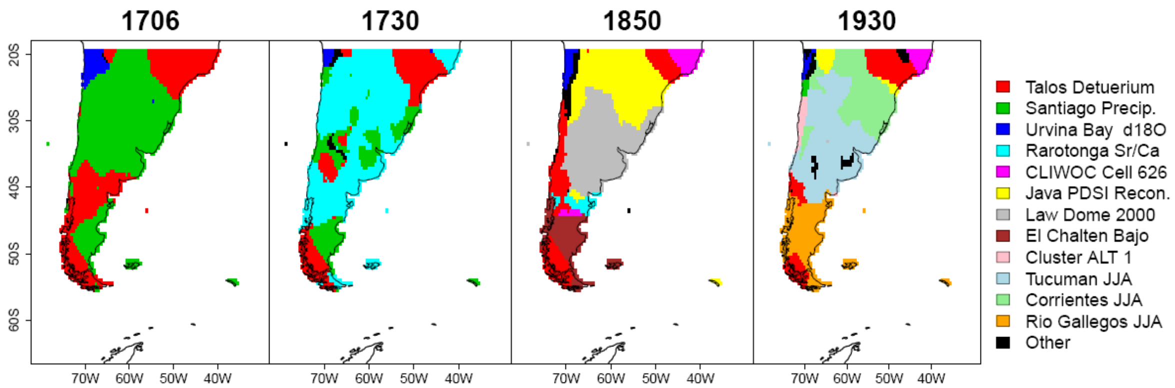

Fig. S18 Same as Fig. S16 but for winter and for the years AD 1706, AD 1730, AD 1850 and AD 1930

7. Supplementary Tables

Table S1 Properties of the SSA tree ring clusters. Lat, Lon and Alt: average latitude, longitude and altitude a.s.l. of the sub-series of the cluster; n: sample depth; sub-series: names of the records that were included into the cluster; Dist.: mean distance (km) between the sub-series; r: average Spearman correlation coefficient between the sub-series. The last two columns indicate, whether the cluster was included into the potential predictor matrix for summer (DJF) and winter (JJA), respectively. The species are listed for each sub-series, if the cluster consists of records from different species.

Name	Lat (S)	Lon (W)	Alt	Start	End	Species	n	Sub-series	Reference	Dist.	r	DJF	JJA
ALT 1	17.67	69.16	4387	1860	1993	POTA	77	Analajchi	Soliz et al. (2009)	70	0.54		X
								Nicolás	Soliz et al. (2009)				
								Huarikunca	Soliz et al. (2009)				
ALT 2	18.46	69.08	4690	1542	2002	POTA	78	Guallatiri Oeste	Soliz et al. (2009)	3	0.91	X	
								Guallatiri Norte	Christie et al.(2009)				
ALT 3	21.55	67.3	4553	1630	1998	POTA	214	Tunupa	Argollo et al. (2004)	143	0.6	X	
								Caquella	Argollo et al. (2004), Soliz et al. (2009)				
								Tapachilca	Soliz et al. (2009)				
								Soniquera	Argollo et al. (2004), Soliz et al. (2009)				
								Uturuncu	Soliz et al. (2009)				
								Granada	Morales et al. (2004)				
NWA 1	23.04	64.392	1170	1833	2002	JGAU	35	El Arrasayal	Villalba et al. (1992)	71	0.53		
								La Meseda	unpublished				
NWA 2	23.68	65.19	2309	1818	2001	CELI	126	Rio Horqueta	Villalba et al. (1992)	296	0.33	X	
						ALAC		Los Toldos	Morales et al. (2004)				
						JGAU		San Jose	unpublished				
						JGAU		Vallecito	unpublished				
NWA 3	24.44	64.74	1189	1826	2002	JGAU	115	Finca las Pichanas	Villalba et al. (1992)	227	0.23		
								Send del Ciervo	Villalba et al. (1992)				
								Cerro los Lobitos	unpublished				
								Los Toldos	Morales et al. (2004)				
NWA 4	24.76	6500	1800	1858	1999	CEAN	73	Finca del Rey	Villalba et al. (1992)	91	0.23	X	
								Rio Blanco	Villalba et al. (1992)				
NWA 5	25.12	65.62	1803	1786	2002	JGAU	170	Rio Horqueta	Villalba et al. (1992)	244	0.16		X
								Rio Bolsas	Villalba et al. (1992)				
								Yala	unpublished				
CAN 1	34.49	70.57	1157	1276	1975	AUCH	165	Alto de las Mesas	La Marche et al. (1979b)	90	0.71	X	
								San Gabriel	La Marche et al. (1979b)				
								Santa Isabel de las Cruces	La Marche et al. (1979b)				
CAN 2	37.84	70.98	1530	1673	1974	ARAR	37	Caviahue	La Marche et al. (1979a)	8	0.66		
								Puente del Agrio	La Marche et al. (1979a)				
CAN 3	38.07	71.21	1570	1640	1975	ARAR	41	Copahue	La Marche et al. (1979a)	64	0.75	X	
								Nalcas	La Marche et al. (1979b)				
CAN 4	38.43	71.3	1483	1704	1994	NOPU	120	Los Barros (Laguna del Laja)	Lara et al. (2001)	212	0.6	X	
								Arroyo Chalahuaco ACC	Schmelter (2000)				
								Las Cuevas (Laguna del Laja)	Lara et al. (2001)				
								Lenga Larga (Laguna del Laja)	Lara et al. (2001)				
CAN 5	38.62	71.6	1640	1787	1996	NOPU	76	Conguillio (Krummholz)	Lara et al. (2001)	0	0.79		
								Conguillio (Lenga media)	Lara et al. (2001)				
CAN 6	38.76	71.35	1460	1232	1983	ARAR	179	Rahue	La Marche et al. (1979a)	143	0.59	X	
								Chenque Pehuen	La Marche et al. (1979a)				
								Primeros Pinos de Alumine	La Marche et al. (1979a)				
								Paso Tromen	Villalba (1990a)				

Table S1 (continued)

								Piedra del Aguila	La Marche et al. (1979b)				
CAN 7	38.88	71.21	1205	1720	1974	ARAR	22	Lago Moquehue	La Marche et al. (1979a)	7	0.72		
								Angostura Lago Alumine	La Marche et al. (1979a)				
CAN 8	39.2	71.19	1125	1676	1989	AUCH	69	Norquinco	Villalba and Veblen (1997)	13	0.54		
								Lago Quillén	Villalba and Veblen (1997)				
CAN 9	39.31	71.22	1246	1407	1989	ARAR	254	Lonco Luan	La Marche et al. (1979a)	46	0.68		
								Estancia Mamuil-Malal	La Marche et al. (1979a)				
								Lago Rucachoroi	La Marche et al. (1979a)				
								Lago Tromen	La Marche et al. (1979a)				
								Estancia Pulmari	La Marche et al. (1979a)				
CAN 10	39.49	70.9	1320	1596	1989	ARAR	44	Rio Kilca	La Marche et al. (1979a)	130	0.44		
						AUCH		Cerro Los Pinos	Villalba and Veblen (1997)				
CAN 11	40.27	72.44	803	1493	2002	PLUV	146	Pozo Mallín	Lara et al. (2008)	89	0.64		
								Lago Ranco	Lara et al. (2008)				
								Puyehue	Lara et al. (2008)				
CAN 12	40.63	71.46	803	1508	1992	AUCH	175	Lago Terraplen	Villalba and Veblen (1997)	381	0.61	X	
								Cerro La Hormiga	Villalba and Veblen (1997)				
								Nahuel - Pan	Villalba and Veblen (1997)				
								Abanico	La Marche et al. (1979b)				
								El Chacay	La Marche et al. (1979b)				
CAN 13	40.88	71.11	1047	1497	2003	AUCH	254	Cerro los Leones	La Marche et al. (1979a)	77	0.67	X	
								Cuyín Manzano	La Marche et al. (1979a), Lara et al. (2008)				
								Confluencia 2	Villalba and Veblen (1997)				
								El Centinela	Villalba and Veblen (1997), Lara et al. (2008)				
								Cerro del Guanaco	Villalba and Veblen (1997), Lara et al. (2008)				
								Rio Minero	Villalba and Veblen (1997)				
								El Mirador	Villalba and Veblen (1997)				
								Pampa del Toro	Villalba and Veblen (1997)				
								Pilcaniyeu	Villalba and Veblen (1997)				
								San Ramón	Villalba and Veblen (1997)				
								Paso del Viento	Villalba and Veblen (1997)				
CAN 14	41.14	71.8	1540	1869	1994	NOPU	152	Paso de las Nubes 1	Villalba et al. (1997)	8	0.7	X	
								Castaño Overo 5	Villalba et al. (1997)				
								Paso Vuriloche	Schmelter (2000)				
CAN 15	41.14	71.8	1355	1566	1991	NOPU	123	Paso de las Nubes 4	Villalba et al. (1997)	2	0.55		
								Castaño Overo 6	Villalba et al. (1997)				
								Castaño Overo 7	Villalba et al. (1997)				
								Castaño Overo 8	Villalba et al. (1997)				
CAN 16	41.15	71.8	1583	1845	1994	NOPU	152	Castaño Overo 3	Villalba et al. (1997)	0	0.69	X	
								Castaño Overo 4	Villalba et al. (1997)				
CAN 17	41.17	71.82	1690	1892	1994	NOPU	55	Castaño Overo 1	Villalba et al. (1997)	5	0.55		X
								Castaño Overo 2	Villalba et al. (1997)				
								Paso Vuriloche	Schmelter (2000)				
CAN 18	41.23	71.5	1550	1634	1994	NOPU	113	Cerro Diego de León DLR	Schmelter (2000)	19	0.61		
								Arroyo Chalahuaco ACR	Schmelter (2000)				
								Cerro Catedral CCR	Schmelter (2000)				
CAN 19	41.25	72.28	1225	1865	1998	NOPU	130	Volcan Yate	Lara et al. (2005)	123	0.52	X	
								Antillanca	Lara et al. (2005)				
CAN 20	41.34	71.81	900	182	1995	FICU	184	Río Frias	Lara et al. (2000)	44	0.65		
								Río Alerce	Villalba (1990b), Lara et al. (2000)				
								Río Horqueta	Lara et al. (2000)				
								La Esperanza	Lara et al. (2000)				
CAN 21	41.56	71.42	670	1796	1989	AUCH	38	Estancia Collun-co	Villalba and Veblen (1997)	365	0.55	X	
								Futaleufú	Villalba and Veblen (1997)				
CAN 22	41.69	71.82	1293	1720	1997	NOPU	123	Futaleufú	Villalba et al. (1998)	142	0.38	X	
								Paso Vuriloche PVM	Schmelter (2000)				
								Paso Vuriloche VVR	Schmelter (2000)				
								Paso de las Nubes VFR	Schmelter (2000)				
CAN 23	41.96	71.81	1215	799	1993	FICU	60	Río Horqueta 2	Lara et al. (2000)	28	0.73		
								Río Motoco	Lara et al. (2000)				
CAN 24	42.47	71.34	765	1677	2002	AUCH	33	Estancia Teresa	La Marche et al. (1979a), Lara et al. (2008)	108	0.55	X	
								El Maiten	La Marche et al. (1979a), Lara et al. (2008)				
CAN 25	42.49	71.82	560	424	1990	FICU	137	Rio Cisne	Lara et al. (2000)	50	0.63		
								Puerto Café	Lara et al. (2000)				
								Río Alejandro	Lara et al. (2000)				
CAN 26	42.5	73.83	750	1585	1987	FICU	60	Tichihue	Villalba (1990a)	0	0.41		
						PLUV		Piuchue	Roig (1991)				
CAN 27	48.59	72.49	819	1699	1996	NOPU	418	Cerro Buenos Aires	Boninsegna et al. (1989)	298	0.29		
								Lago Fontana	ITRDB series arge037				
								Cochrane	Lara et al. (2005)				
								El Chalten medio	Srur et al. (2008)				
								Campo Chileno	Aravena et al. (2002)				
CAN 28	50.88	72.7	945	1840	1996	NOPU	62	Contreras E	Aravena et al. (2002)	33	0.31	X	
								Campo Torres	Aravena et al. (2002)				
CAN 29	51.15	73.29	650	1734	1996	NOPU	100	Cerro Ferrier A	Aravena et al. (2002)	1	0.81		
								Cerro Ferrier B	Aravena et al. (2002)				
CAN 30	53.08	69.86	246	1852	1996	NOPU	128	Monte Gallina	Aravena et al. (2002)	199	0.41		X
								Estancia las Flores	Aravena et al. (2002)				
CAN 31	54.33	68.36	365	1703	1996	NOBE, NOPU	143	A. Isla Grande 2	Boninsegna et al. (1989)	45	0.56		X
						NOPU		Cerro Balseiro	Aravena et al. (2002)				
						NOPU		Campo XX inferior	Aravena et al. (2002)				
						NOPU		Campo XX medio	Aravena et al. (2002)				
SAN 1	54.34	67.9	217	1769	1986	NOBE, NOPU	125	A. Isla Grande 1	Boninsegna et al. (1989)	61	0.65		
						NOPU		Estancia san Justo	Boninsegna et al. (1989)				
						NOPU		Lago Yehuin	Boninsegna et al. (1989)				
SAN 2	54.38	68.64	567	1845	1996	NOPU	156	Aserradero S	Aravena et al. (2002)	123	0.61	X	
								Cerro Pascua	Aravena et al. (2002)				

Table S1 (continued)

								Campo XX Krummholz	Aravena et al. (2002)				
SAN 3	54.48	67.6	233	1761	1986	NOPU	116	Estancia Carmen	Boninsegna et al. (1989)	54	0.77		
								Estancia Maria Cristina	Boninsegna et al. (1989)				
								Rio Claro	Boninsegna et al. (1989)				
SAN 4	54.65	67.8	150	1724	1984	NOBE, NOPU	66	Rio Pipo	Boninsegna et al. (1989)	18	0.3		X
						NOPU		Valle de Andorra	Boninsegna et al. (1989)				
SAN 5	54.72	67.62	513	1725	1986	NOPU	131	Estacion Microondas	Boninsegna et al. (1989)	34	0.63		X
						NOBE		Paso Garibaldi	Boninsegna et al. (1989)				
						NOBE, NOPU		Lago Escondido	Boninsegna et al. (1989)				
						NOBE		Rio Moat	Boninsegna et al. (1989)				
SAN 6	54.77	64.5	40	1731	1986	NOBE	49	Bahia York	Boninsegna et al. (1989)	26	0.63	X	
								Bahia Crossley	Boninsegna et al. (1989)				
SAN 7	54.93	67.47	240	1766	1996	NOBE	59	Estancia Harberton	Boninsegna et al. (1989)	17	0.73		
						NOPU		Cerro Bandera Abajo	Aravena et al. (2002)				
SAN 8	54.93	67.81	542	1776	1996	NOPU	89	Aserradero NW	Aravena et al. (2002)	20	0.61		
								Cerro Bandera Krummholz	Aravena et al. (2002)				
								Cerro Vallerino Krummholz	Aravena et al. (2002)				

Table S2 Properties of the SSA tree ring series, which were not included into a cluster. The coordinates and altitudes of the sites, beginning and end years, species, sample depths (n) and references of the series are shown. The last two columns indicate, whether the record was included into the potential predictor matrix for summer (DJF) and winter (JJA), respectively.

SiteName	Lat (S)	Lon (W)	Alt	Start	End	Species	n	Reference	DJF	JJA
Purisima, Bolivian Amazon	10.92	65.67	250	1905	2001	CEOD	64	Brienen and Zuidema (2005)		
Concepción, Ñuflo de chavez	16.37	62.13	244	1861	2005	CEMI	35	unpublished (L. Lopez pers. comm.)		
Serke	17.43	69.33	4440	1955	2002	POTA	15	Soliz et al. (2009)		
La Meseda	23.00	65.02	1600	1826	1999	CELI	23	unpublished		
Quebrada de Humahuaca	23.17	65.33	3450	1886	2001	PRFE	62	Morales et al. (2004)	X	
Rio Sala and Popayan	24.60	64.60	700	1881	2002	JGAU	39	Villalba et al. (1992)[a]		
Los Laureles	25.12	65.55	1650	1863	1979	JGAU	12	Villalba et al. (1992)		
Dique Escaba	27.70	65.78	900	1887	1985	JGAU	24	Villalba et al. (1992)	X	
Palo Colorado 1	32.17	71.00	74	1839	2003	MYEX	18	unpublished (A. Maldonado, pers.comm)	X	
Palo Colorado 2	32.17	71.00	74	1917	2004	MYEX	10	unpublished (A. Maldonado, pers.comm)		
El Asiento	32.48	70.82	1800	1280	1972	AUCH	65	La Marche et al. (1979b)		
Bonilla	32.68	69.12	2800	1941	1985	ADUS	13	Roig and Boninsegna (1990)		
Alto los Manantiales	32.72	69.08	3100	1827	1986	ADHO	19	Roig and Boninsegna (1990)		
Vilches	35.60	71.03	1530	1880	1996	NOPU	49	Lara et al. (2001)	X	
Huinganco	37.07	70.60	1400	1635	1975	AUCH	34	La Marche et al. (1979a)		
Petronquines (Laguna del Laja)	37.48	71.32	1690	1833	1995	NOPU	24	Lara et al. (2001)		
Caramavida	37.68	73.17	900	1548	1972	ARAR	20	La Marche et al. (1979b)		
Volcan Lonquimay	38.38	71.57	1510	1702	1975	ARAR	47	La Marche et al. (1979b)		
Pino Hachado	38.63	70.75	1400	1541	1974	ARAR	31	La Marche et al. (1979a)		
Conguillio (Lenga abajo)	39.22	71.167	1490	1774	1996	NOPU	55	Lara et al. (2001)	X	
Lago Rucachoroi	40.12	71.43	1330	1691	1976	AUCH	26	La Marche et al. (1979a)		
Piedra Tromphul	40.13	73.52	1060	1877	1989	AUCH	10	Villalba et al (1998b)		
Hueicolla	40.33	71.23	800	1937	1975	PLUV	14	La Marche et al. (1979b)		
Chapelco	40.67	71.25	1700	1822	1985	NOPU	29	ITRDB series arge029		
Paso Cordova	41.12	71.80	1890	1760	1986	NOPU	37	ITRDB series arge050		
Paso de las Nubes 3	41.17	71.48	1320	1848	1991	NOPU	20	Villalba et al. (1997b)		
Cerro Catedral	41.17	71.93	1890	1922	1994	NOPU	29	Schmelter (2000)		
Glaciar Frias	41.25	71.75	1200	1802	1985	NOPU	21	Villalba et al. (1990)	X	
Castaño Overo Maduro	41.27	71.62	1100	1742	1982	NOPU	21	ITRDB series arge027		
Cerro Diego Leon	41.55	72.60	1700	1903	1994	NOPU	53	Schmelter (2000)		
Lenca	41.67	71.42	875	-499	1987	FICU	43	Lara and Villalba (1993)		
Rio Foyel	43.00	72.50	1200	1803	1982	PLUV	22	Roig (1991)		
Santa Lucia	44.65	71.70	540	1646	1986	PLUV	60	Szeicz et al. (2000)	X	
Cisnes	45.92	71.75	1100	1811	1997	NOPU	54	Lara et al. (2005)		
Balmaceda	48.50	72.50	600	1828	1988	NOPU	18	ITRDB series arge023		X
O Higgins	49.37	72.90	1200	1892	1999	NOPU	24	Lara et al. (2005)	X	
El Chalten bajo	49.37	72.93	760	1807	2003	NOPU	100	Srur et al. (2008)		X
El Chalten alto	50.42	72.17	1100	1917	2002	NOPU	44	Srur et al. (2008)		
Valle Ameghino	50.80	72.60	700	1743	1997	NOPU	41	Masiokas and Villalba (2004)		
Contreras W	53.15	71.03	920	1831	1996	NOPU	62	Aravena et al. (2002)		
Cancha de Ski (Punta Arenas)	53.20	72.17	600	1911	1996	NOPU	38	Aravena et al. (2002)		
Monte Grande	53.37	71.22	300	1761	1988	NOPU	17	ITRDB series arge049		X
Monte Azul	53.50	71.17	500	1782	1996	NOPU	48	Aravena et al. (2002)		
Peninsula Brunswick	54.52	66.17	100	1760	1988	NOPU	17	Boninsegna et al. (1989)		
Rio Malenguena	54.78	68.38	15	1775	1986	NOPB	42	Boninsegna (1988)		
Cerro Martial	54.83	64.37	550	1798	2003	NOPU	37	Mundo et al. (2007)		
Puerto Parryn	54.83	65.20	20	1760	1986	NOBE	25	Boninsegna et al. (1989)		
Bahia del Buen Suceso	54.90	68.00	35	1751	1986	NOBE	17	Boninsegna et al. (1989)		
Cerro Vallerino Abajo	38.63	71.60	300	1787	1996	NOPU	55	Aravena et al. (2002)		

[a] And additional unpublished samples

Table S3 Proxy records from other archives, which were available for the reconstructions. The last two columns indicate whether the record was included into the potential predictor matrix for summer (DJF) and winter (JJA), respectively.

SiteName	Archive	Lat (S)	Lon (W)	Start (AD)	End (AD)	Reference	DJF	JJA
Cariaco Basin	Marine Sediment	-10.75	64.77	1165	1990	Black et al. (2007)	X	X
Secas d13C	Coral	-7.00	82.05	1707	1984	Linsley et al. (1994)		
Secas d18O	Coral	-7.00	82.05	1707	1984	Linsley et al. (1994)		
F-T IDPO index	Coral	0.02	180.00	1650	2004	Linsley et al. (2008)		
Urvina, Galapagos Islands	Coral	0.03	91.23	1607	1981	Dunbar et al. (1994)		X
Java PDSI reconstruction	Tree rings / Coral	7.00	-111.00	1787	2003	D'Arrigo et al. (2006)		X
106KL off Peruvian coast	Marine Sediment	12.05	77.67	-13550	2000	Rein (2007)		
Quelccaya accumulation	Ice Core	13.93	70.83	488	2003	Thompson et al. (2000, 2006)	X	X
Quelccaya d^{18}O	Ice Core	13.93	70.83	488	2003	Thompson et al. (2000, 2006)	X	
Illimani deuterium	Ice Core	16.65	67.78	898	1998	Ramirez et al. (2003), Vimeux et al. (2009)		
Illimani NH_3 temperature reconstruction	Ice Core	16.65	67.78	362	1989	Kellerhals (2008)	X	
Great Barrier Reef Ba/Ca	Coral	18.00	-146.00	1758	1998	McCulloch et al. (2003)	X	
Avaiki	Speleothem	19.00	169.83	1829	2001	Rasbury and Aharon (2006)		
Potosi precipitation index	Documentary	19.58	65.75	1585	2006	Gioda and Prieto (1999a,b), Neukom et al. (2009)		
Great Barrier Reef coral luminescence	Coral	20.00	-147.00	1631	2005	Lough (2007)		
Rarotonga	Coral	21.23	159.83	1726	1996	Linsley et al. (2000)		X
New Caledonia d^{18}O	Coral	22.48	-166.45	1657	1992	Quinn et al. (1998)	X	
New Caledonia d^{13}C	Coral	22.48	-166.45	1657	1992	Quinn et al. (1998)		
Campinas	Instrumental	23.00	47.12	1890	2003	Vargas and Naumann (2008)	X	X
Ifaty, Madagascar d^{13}C	Coral	23.15	-43.58	1659	1995	Zinke et al. (2004)		
Ifaty, Madagascar d^{18}O	Coral	23.15	-43.58	1659	1995	Zinke et al. (2004)		
Tucuman	Instrumental	26.80	65.20	1891	2000	Vargas and Naumann (2008)	X	X
Dulce River runoff index	Documentary	27.00	65.00	1750	1980	Herrera et al. (2003), Neukom et al. (2009)		
Tucuman precipitation index	Documentary	27.03	65.00	1548	2006	Prieto et al. (2000), Neukom et al. (2009)		
Corrientes	Instrumental	27.43	58.73	1894	2004	Vargas and Naumann (2008)	X	X
Santiago del Estero precipitation index	Documentary	27.77	64.27	1750	2006	Herrera et al. (2003), Neukom et al. (2009)		
Abrolhos d^{13}C	Coral	28.45	-113.77	1794	1993	Kuhnert et al. (1999)	X	

Table S3 (continued)

Abrolhos $d^{18}O$	Coral	28.45	-113.77	1794	1993	Kuhnert et al. (1999)		
Parana River runoff index	Documentary	30.00	60.00	1590	1994	Prieto (2007), Neukom et al. (2009)		
Santa Fe and Corrientes precipitation index	Documentary	30.00	60.00	1590	2006	Prieto (2007), Neukom et al. (2009)		
Cordoba	Documentary	31.00	64.00	1700	2006	Prieto and Herrera (2001), Neukom et al. (2009)	X	
Mendoza River runoff index	Documentary	32.00	68.00	1601	2000	Prieto et al. (1999a), Neukom et al. (2009)		
Mendoza precipitation index	Documentary	32.00	68.00	1600	2000	Prieto et al. (2000), Neukom et al. (2009)		
Central Andes snow depth	Documentary	33.00	70.00	1760	1996	Prieto et al. (1999b), Neukom et al. (2009)	X	
Central Andes snow days	Documentary	33.00	70.00	1885	1996	Prieto et al. (2001a, b)		X
Santiago de Chile precipitation index	Documentary	33.38	70.78	1540	2006	Taulis (1934), Neukom et al. (2009)		X
Laguna Aculeo	Lake Sediment	33.83	70.90	857	2003	von Gunten et al. (2009)	X	
New Zealand temperature reconstruction	Tree rings	43.33	-170.50	900	1999	Cook et al. (2002)	X	
Rio Gallegos	Instrumental	51.98	69.45	1896	2004	Vargas and Naumann (2008)	X	X
James Ross Island	Ice Core	64.37	58.13	1791	2000	Aristarain (2004)	X	
Law Dome 2000	Ice Core	66.83	-112.83	1800	1999	van Ommen et al. (2004)		X
Dolleman	Ice Core	70.97	61.55	1761	1970	Fisher (2002)		X
Dyer Plateau 1	Ice Core	71.12	65.45	1761	1970	Fisher (2002)		
Talos	Ice Core	72.80	-159.10	1217	1996	Stenni et al. (2002)		X
Gomez	Ice Core	73.60	70.35	1855	2006	Thomas et al. (2008)	X	
Dronning Maud Land	Ice Core	75.00	0.00	1800	1999	Graf et al. (2002)		
ITASE 2000 5	Ice Core	77.67	124.00	1800	1999	Schneider et al. (2006)		
ITASE 2000 1	Ice Core	79.63	111.38	1800	1999	Schneider et al. (2006)		
Dyer Plateau 2	Ice Core	84.00	-43.00	1761	1970	Fisher (2002)		
Peru El Niño index (documents from various locations in northern Peru)	Documentary			1525	1990	García-Herrera et al. (2008); 20th century data from Quinn and Neal (1992)		X
Ship log data (South Atlantic, various locations)	Documentary			1750	2002	Garcia-Herrera et al. (2005), Küttel et al. (2009)		X
SOI reconstruction (N-American and Indonesian trees)	Tree rings			1706	1977	Stahle et al. (1998)		X

Table S4 Standard deviations (in °C) of the spatial means of the SSA sub-regions, averaged over the 1901-1995 period in the reconstructions and the instrumental data (CRU).

	Summer		Winter	
	Std.dev. (Recon)	Std.dev. (CRU)	Std.dev. (Recon)	Std.dev. (CRU)
South Patagonia	0.73	0.67	0.74	0.65
North Patagonia	0.67	0.60	0.69	0.65
Central Chile	0.66	0.57	0.58	0.54
Subtropical SSA	0.37	0.40	0.70	0.68